Introduction

There are rich varieties of oscillating systems with more or less external driving forces in all disciplines[1,2]. Although the physical objects even the physical interactions may appear to be unrelated for different systems possessing similar oscillation characteristics, the behavioral similarity from a dynamical point of view can provide invaluable insight for investigators modeling these systems.

By examining the general dynamics with discrete time algorithm, we review first the nonlinear phase locking behavior of a macroscopic superconductive driven oscillation[3]. With the similar phase locking dynamics another collective quantum electromagnetic phenomenon in macroscopic scale, the quantized Hall effects, can be realized. The phase slip picture of vortex has been used to model the macroscopic dynamics of the Josephson oscillation. If a coordinate transformation from the flowing vortex to the fixed flux is considered, an analogy between the driven Josephson oscillation and the quantized Hall effects can be made.

Another oscillating system investigated can be categorized to classical kinetics of a macroscopic material system. Reflection High Energy Electron Diffraction (RHEED) has been widely used in monitoring and controlling Epitaxy film growth[4,5]. Since the electron beam travels in the traverse direction of the depositing materials, RHEED provided exclusive convenience for in-situ detecting the surface morphological condition during the film growth. The low glancing angle and high energy of the electron beam made possible in-situ monitoring the few topmost layers of the deposited film.

One of the most valuable applications of the RHEED in-situ monitoring is to reveal the layer by layer growth of Epitaxy film growth. Although the detailed diffraction mechanism is still remained to be concluded, the evident correlation

PDF created with FinePrint pdfFactory trial version http://www.fineprint.com

between the period of the RHEED intensity oscillation and the layer counts of film growth has proven to be one of the most precise tools for preparing good quality films[6-9]. The oscillation of the RHEED intensity can be regarded as a competition between the deposition of source material and the diffusion of the adatoms. In order to gain a clearer vision for the oscillating characteristics, we conducted a series of RHEED intensity analysis on the annealing behaviors of the laser-deposited Strontium Titanate films. From quantitative analysis of the temporal and temperature annealing data, a direct relation between the RHEED intensity and the kinetic law of activated diffusion was found. The results not only suggested a convenient tool for characterizing the kinetics of material, but also revealed more about the kinetics itself.

2

References

[1] For example, "Nonlinear Dynamics and Chaos", S.H. Strogatz, Addison-Wesley, 1994.

[2] "Chaos in Nonlinear Oscillators", M. Lakshmanan and K. Murali, World Scientific, 1996.

[3] R.L. Kautz, Rep. Prog. Phys. Vol. 59, 935 (1996), K.K. Likharev, "Dynamics of Josephson Junctions and Circuits", Gordon and Breach Science Publishers (1986), Y.H. Gao, Doctoral dissertation, National Chiao-Tung University, Taiwan. (1985).

[4] "Applied Rheed: Reflection High-Energy Electron Diffraction During Crystal Growth", Braun, Wolfgang, Springer-Verlag Berlin and Heidelberg GmbH & Co. KG, 1999.

[5] "Reflection High-Energy Electron Diffraction and Reflection Electron Imaging of Surfaces", Edited by P. K. Larson and P. J. Dobson, Plenum Press New York and London, 1988.

[6] J.J. Harris,B.A. Joyce,P.J. Dobson, Surf. Sci. 103, L90 (1981).

[7] C.E.C. Wood, Surf. Sci. 108, L441 (1981).

[8] J.M. van Hove, C.S. Lent,P.R. Pukite,P.I. Cohen, J. Vac. Sci. Technol. B 1, 741 (1983).

[9] J.H. Neave,B.A. Joyce,P.J. Dobson,N. Norton,Appl..Phys. A 31, 1 (1983).

Chapter 1   Phenomenology of Macroscopic Quantum Phase Locking

1-1   rf-biased ac Josephson Effect and Quantized Hall effects

When the applied current is larger than the critical current for a superconductive Josephson junction, there will be a voltage drop V between the two electrodes of the junction along with a macroscopic quantum oscillation with the frequency $w_J = \dfrac{2eV}{\mathbf{h}}$. The superconductivity reveals its condensed quantum nature by the paired charges as well as the Planck's constant. If the junction is further exposed to a microwave irradiation with frequency w_{rf}, the voltage drop can be found [1,2] as quantized Shapiro steps of

$$V = \frac{n}{m}\frac{\mathbf{h}}{2e}w_{rf}, \tag{1}$$

where n/m represents a simple rational number. Fig. 1-2. shows the first observation of the fractional Shapiro steps. As the applied current increases to the critical current, the voltage drop displays a quantized "devil's staircase" fractal structure.
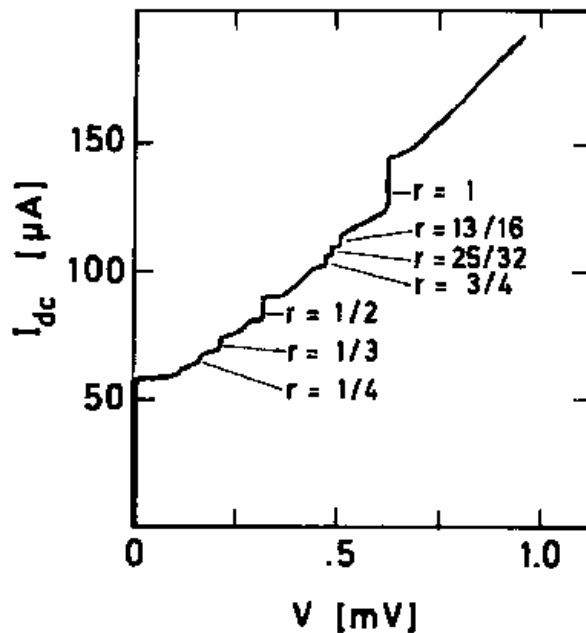

Fig. 1-1. Fractional Shapiro steps of a rf-irradiated Josephson point junction[2].

4

Another macroscopic quantum system showing the intriguing devil's staircase structure is the quantum Hall effects[3,4]. The same time as the longitudinal Hall current becomes perfectly conducting, the transverse Hall resistance R_H in the Quantum Hall effect can be quantized in units of $\dfrac{h}{e^2}$:

$$R_H = \frac{1}{n}\frac{h}{e^2},\qquad (2)$$

the filling factor n is an integer for the integer quantum Hall effect (IQHE) or a fractional number for the fractional quantum Hall effect (FQHE). In Fig. 1-3., an example of the FQHE demonstrate the devil's staircase structure as the magnetic flux density was varied[5].
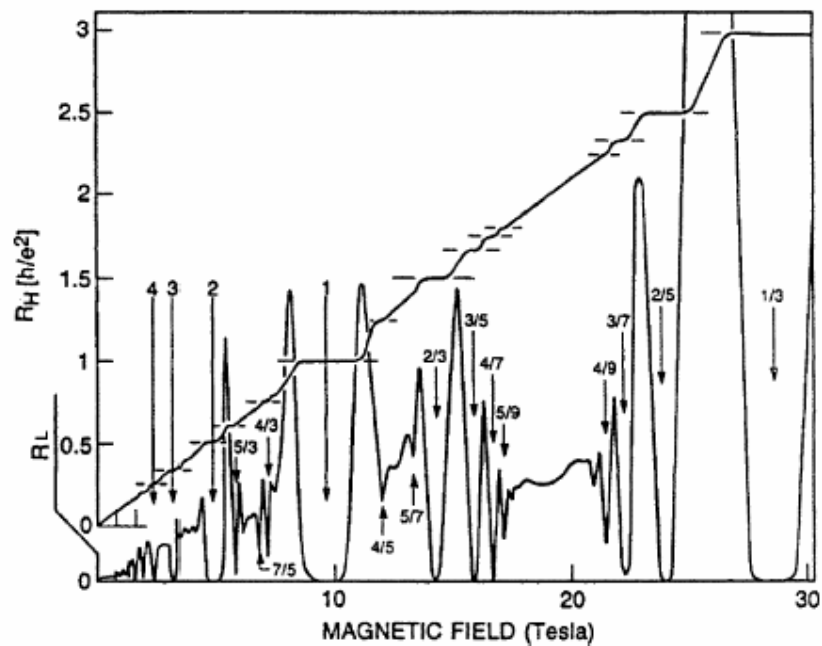

Fig. 1-2. Fractional Quantized Hall effect showing the devil's staircase structure of the Hall resistance versus varied field and the perfect conductivity of longitudinal current[5].

Interestingly, we see from a simple dimensional check that the quantized Hall

resistance can be expressed as $\dfrac{h}{e^2}$ multiplied by the frequency ratio of a

Josephson-type oscillation to an electron wave.

For those nonlinear oscillation systems difficult to be solved analytically, one finds computer simulation particularly useful. In the appendix, the well known Duffing oscillator has been used to demonstrate basic methodology of nonlinear dynamics. To understand the nonlinear resonance in a more general context, one also finds that the phase-locking can be modeled by a discrete time map.

For the ac Josephson oscillation, Jensen and Bak[6,7] illustrated that by physically taking the period of external driving as the "stroboscopic" time period of the Poincaré section, the circle map

$$\Theta_{n+1} = \Theta_0 + \Omega + g(\Theta_n) \qquad (3)$$

may well display all the key features of the dissipated phase locking behavior observed in the numerical treatment of the ODE system of a driven oscillation. In the map (3), n is the number of times of Poincaré sectioning, $g(\Theta_n)$ is a function representing the nonlinear interaction and Ω is the rotation parameter related to the coefficients of the pendulum equation. In the parameter regions where phase locking behavior appears, function $g(\Theta_n)$ was found topologically equivalent to a sine function and can be chosen for convenience to be $-(K/2p) \cdot \sin(2p\Theta_n)$, where K represents the coupling strength.

To illustrate the phase locking dynamical behavior of the circle map, one defines the winding number

$$W = \lim_{n \to \infty} \frac{\Theta_n - \Theta_0}{n}. \qquad (4)$$

Since each iterate in the map corresponds to one period of the external drive, the winding number measures the frequency ratio between the system and the external force as the steady state is achieved.

7

At the weak nonlinear perturbation limit $K \sim 0$, from (1) and (2) we have $W \sim \Omega$. The winding number thus traces up the diagonal on the (Ω, W) parameter diagram, and Ω trivially represents the frequency ratio at the weak perturbation limit. When $K > 0$, the smooth diagonal line changes into a staircase structure. At the Ω regions corresponding to the plateaus, phases are locked and the frequency ratios are found to be rational numbers. Whereas at those Ω regions between plateaus, the system is in unlocked quasiperiodic states, and the frequency ratios are irrational numbers. When $K = 1$, the Ω-W staircase develops a complete structure in which the total projection length of the quasiperiodic regions on the Ω axis turns out to be zero. In other words, the full range of Ω is occupied by phase locked regions. Such a peculiar structure is designated as the devil's staircase, see Fig. 1-3. When $K > 1$, the deterministic chaos appears due to the interaction of the neighboring steps.
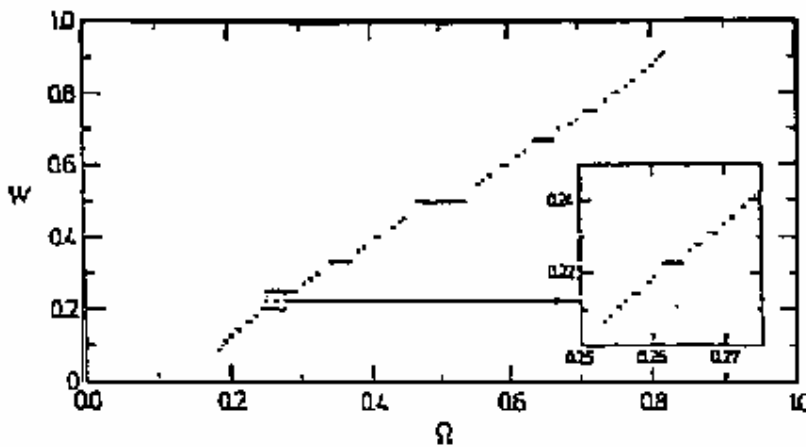

Fig. 1-3. The Devil's staircase of a circle map. Winding number W vs. rotation

parameter Ω for the circle map at $K=1$. The inset shows the self-similar

fractal nature of the staircase. (Jensen, Bak and Bohr, Ref. [7].)

References

[1] S. Shapiro, Phys. Rev. Lett., **11,** 80 (1963).

[2] V.N. Belykh et. al., Phys. Rev. B. **16,** 4860 (1978).

[3] R.E. Prange et. al., The Quantum Hall Effect, Springer-Verlag (1990).

[4] T. Chakraborty et. al., The Quantum Hall Effects, 2nd edition, Springer-Verlag (1995).

[5] G.S. Boebinger et. al., Phys. Rev. B. **32**, 4268 (1985).

[6] M. H. Jensen *et. al.,* Phys. Rev. Lett. **50,** No. 21, 1637 (1983).

[7] P. Bak *et. al.,* Solid State Comm. **51.** No. 4, 231 (1984). For more detailed discussions, also see: Phys. Rev. A. **30**, No. 4, 1970 (1984).

Chapter 2   Driven ac Josephson effect and Quantum Hall Effects-

A Macroscopic Quantum Phase-Locking Analogy

The Josephson Resistively and Capacitively Shunted Junction (RCSJ) system is one of the most investigated nonlinear dynamical system capable of showing a unique macroscopic phase-locking behavior. Instead of considering RCSJ equation as merely a phenomenological circuit model, we investigate the quantum aspects embedded in it. Following de Broglie's relativistic derivation, we consider a covariant analogy between the Josephson relation and de Broglie relation. Fundamental properties including Lorentz invariance are pointed out. Based on the assumption of two-frequency locking macroscopic quantization, a possible connection between the Quantized Hall effects and the driven ac Josephson effect is proposed.

2-1 ac Josephson Effects and RCSJ Circuit Model

In the r.f-driven ac Josephson effect, the energy difference between the two sides of the junction barrier can be rationally quantized to Shapiro steps [1,2]:

$$\Delta E = qV = \frac{n}{m}\mathbf{h}w_{rf}, \tag{1}$$

where $q = 2e$ is the electric charge of the superconducting Cooper pairs, V is the voltage drop across the junction, $\mathbf{h}$ denotes Planck's constant $h/2p$, w_{rf} represents the frequency of the driving field and n/m implies a simple rational number including an integer or a fractional number. This energy quantization has been successfully simulated by the following resistively and capacitively shunted junction (RCSJ) model[3, 4].

The Josephson relations[5] includes the energy-frequency relation:

$$qV = \mathbf{h}\frac{dj}{dt}, \tag{2}$$

where j represents the macroscopic quantum phase difference across the junction, and the nonlinear current-phase relation typically expressed by a sine function:

$$I_J = I_c \sin j \tag{3}$$

where I_J is the Josephson current and I_c the critical current. Resistively and Capacitively Shunted Junction (RCSJ) model treats the junction as composed of a capacitor, a resistor and the Josephson junction in parallel. The current conservation (KCL) law across the junction can be expressed as a differential equation:

$$C\frac{\mathbf{h}}{q}\frac{d^2 j}{dt^2} + \frac{1}{R}\frac{\mathbf{h}}{q}\frac{dj}{dt} + I_c \sin j = I_{dc} + \left|I_{rf}\right|\cos(w_{rf}t) \tag{4}$$

where the capacitance C and the resistance R are effective parameters, I_{dc} represents the applied dc current and $\left|I_{rf}\right|\cos(w_{rf}t)$ represents the periodic driving current from

11

rf field. This non-autonomous second order equation can also be written as a 3-dimensional state flow:

$$\frac{dj}{dt} = \frac{\Delta E}{\mathbf{h}}, \tag{5}$$

$$\frac{d(\Delta E)}{dt} = \frac{q}{C}(I_{dc} + \left| I_{rf} \right| \cos q - \frac{\Delta E}{qR} - I_c \sin j), \tag{6}$$

and

$$\frac{dq}{dt} = w_{rf}, \tag{7}$$

where $q = w_{rf} t$ denotes the phase of the driving field. The RCSJ flow has been intensively studied as a model system demonstrating various typical nonlinear dynamical behaviors including chaotic, quasi-periodic and periodic states of a forced dissipative oscillation. The quantized energy difference (1) can be modeled as the result of the frequency-locked state

$$\frac{<\Delta j / \Delta t>}{w_{rf}} = \frac{n}{m}, \tag{8}$$

where the rational number *n/m* represents the locked frequency ratio of the Josephson oscillation to the driving field.

This dynamical system was generally regarded as a classical phenomenological recipe to describe Shapiro steps as well as other I-V characteristics of the Josephson junction under microwave irradiation. The intrinsic quantum nature revealed by the Planck's constant may have been attributed to the derivation proving the Josephson relations (2) and (3) and the phase difference j.

Physicists haven't shown serious concerns for the quantum nature in the phase-locking mechanism even though it apparently provided a Planck's constant-involved quantization procedure of energy. Actually from experiments[6] the precision of this macroscopic quantization can be higher than the energy quantization in those microscopic quantum systems modeled by the QED framework.

12

In the following work we intend to make discussions on the possibility that the time evolution of the Josephson phase difference such as the phase-locking behavior of the 3-dimensional dynamical system can be seen from an alternative macroscopic quantum dynamics point of view. The Josephson frequency relation with the Planck's constant is to be considered as a postulate, playing somewhat a similar conceptual role of the Einstein-de Broglie energy-frequency relation in microscopic quantum rules. In other words, the Josephson phase difference is postulated to be a dynamical variable, although emerged from a condensed many-particle system. To imagine the RCSJ state flow of Kirchhoff's current law as a theoretical system of quantum nature, one faces at least two practical issues. One is the capability of this deterministic system to demonstrate the unpredictable nature of a quantum event, the other is the way it discretizes physical quantities. Qualitatively, for a nonlinear dissipative system as the RCSJ flow, ordered chaos may be found with various parameter combinations. Whether the outcome distribution of the evolution can be linked to quantum probabilistic distributions is still an unasked question. However, it has not been presented as a proved result that the deterministic chaotic events can not provide any statistical distribution of quantum mechanical.

Another significant feature of a quantum dynamical rule is the discretization of physical quantities. If we consider the electrical potential quantization revealed by the Shapiro steps as a quantum-dynamical quantization, we are actually suggesting that the two frequency-locking mechanism is able to provide a quantization theoretical framework in which the index of quantum levels are given by the locked frequency ratio.

In the historical development of quantum theory, an intimate correlation between the quantum phase and the Action, or the time integral of Lagrangian, has always been playing an important role in the quantization procedure. If we take a look at the early development of the quantum mechanics, the Bohr-Sommerfeld-Wilson (BSW) quantization condition

$$\oint_{2p} dS = nh \tag{9}$$

states that for a quantum particle, the action integration $\int dS$ such as $\int p dq$ over one period of the cyclic coordinate is equal to an integral multiple of the Planck's constant h. Although this rule can hardly be proved as a general principle of all quantum systems, it did provide an elegant tactics bridging the gap between the quantum and classical regimes, at least for a bounded single particle.

Now, if we define a "phase-ratio action" for the RCSJ flow:

$$S_{j/q} = h\frac{dj}{dq} \tag{10}$$

it turns out that the rational frequency-locking

$$\frac{<\Delta j / \Delta t>}{w_{rf}} = \frac{n}{m} \tag{11}$$

results in a locked action just like the BSW quantization condition:

$$S_{j/q} = \frac{n}{m}h . \tag{12}$$

Furthermore, if we postulate an equivalency between the "phase-ratio" action and the action integral of BSW condition (9), and designate an "action variable" as

$$J = S_{j/q} / 2p , \tag{13}$$

we are allowed to rewrite the frequency-locked energy evolution equation (6) of RCSJ flow for a conserved energy difference as

14

$$\frac{dJ}{dt} = \frac{d(\Delta E)}{w_d dt} = 0. \tag{14}$$

We see that the set of equations (14) and (7) bears an intriguing resemblance of the classical action-angle variable formalism for a single periodic motion.

To imagine the Kirchhoff's current law as a dynamic law of quantum nature, we consider a direct analogy between the Josephson oscillation and a quantized oscillator. In fact, a correspondence between the Josephson oscillation and the quantized electromagnetic field can be seen in the comparison between the Josephson relations with the Maxwell equations. The Josephson voltage-frequency relation can be mapped to the Faraday's law once the Josephson phase difference is assumed to measure the number of passing magnetic flux quanta at a fixed position. The Josephson nonlinear current-phase relation provides a temporal version of the Ampere's law, which is a spatial-temporal relation of flux and circular current.

For a specific Josephson junction, parameters in the RCSJ flow such as R and C, or even forms of functions such as $\sin j$ for I_J and $\cos q$ for I_{rf} may all be subject to change due to different experimental situations. However we consider that some topological properties of our major concern, which qualitatively differentiate all RSJ flow like system from the Hamiltonian system, would be universal. Firstly, the stationary action, i.e., the state space area conservation of periodic RSJ flows, comes from a state space-contracting evolution of a dissipative three-dimensional system, in which the dimensionality "three" would be the minimum state space dimensions needed for a flow to be able to evolve chaotically. While for the 2-dimensional Hamiltonian system the action remains constant just because it is assumed to be conserved in the first place. In addition, the dimension-reducing dissipation also provides a physical explanation for the adiabatic invariant nature of quantized quantities. In other words, for a dissipative dynamical system an ensemble of different

15

initial states tends to evolve into a same attractor, either phase-locked or chaotic, provided that the ensemble of initial points can be covered by the same basin of attraction. Another noteworthy difference is the nonlinearity of RSJ like flows. Since the structured randomness of quantum events is expected to be simulated by the deterministic chaotic state evolution, the linearity of probabilistic quantum mechanics in the superposition principle of the wave function is no longer present as a central notion. Instead, the nonlinearity of the functions of phases j and q, symbolizing the periodicity of phases, would always be necessary for demonstrating chaotic behavior and stands for the nonlinear reality of the physical model.

To explore the discretization of physical quantities, we recall a connection between quantum systems and classical ones, the canonical conjugation relations. Not only an action product of two conjugated variables, such as energy and time, appears to be the basic unit for quantization, but also the corresponding variables of two conjugated pairs, such as energy and momentum or time and space, make up a building block 4-vector in the relativity theory. Taking into consideration these two facts, we expect to find some fundamental guideline for a quantization program by exploring the conjugated properties embedded in the RSJ state flow. For instance if we manage to obtain, within the universal phase-locking scheme of the RSJ flow, a connection between energy quantization and momentum quantization, we would be in a good position to find some correspondence rule showing the classical relation of energy and momentum. As a matter of fact, such a connection has been initiated by Louis de Broglie in his Lorentz invariant derivation of momentum-wave number relation[7].

In de Broglie's work, he argued that if one observes a propagating quantum wave from its own frame O', he would obtain a pure temporal state evolution with the Einstein energy-frequency relation:

16

$$dj' = w'dt' = \frac{E'}{\mathbf{h}}dt' \qquad (15)$$

where j' is the quantum phase and w' denotes the frequency. On the other hand, the state evolution of the traveling wave observed from a "rest" reference frame O would contain a space-dependent part

$$dj = wdt - kdx, \qquad (16)$$

where all variables are subjected to the rest frame and k represents the quantum wave vector. Since it is straightforward to postulate that the phase changes observed from these two frames are identical, we can equalize dj obtained from (16) with dj' obtained from (15):

$$w'dt' = wdt - w\frac{v}{c^2}dx \qquad (17)$$

and find that the wave vector k equals wv/c^2. Taking into account the equality of the relativistic energy and the quantum energy, we have the momentum P for the matter wave quantized as $\mathbf{h}k$ since

$$P = \frac{m'v}{\sqrt{1-(\frac{v}{c})^2}} = \frac{(\mathbf{h}w'/c^2)v}{\sqrt{1-(\frac{v}{c})^2}} = \mathbf{h}w\frac{v}{c^2} = \mathbf{h}k . \qquad (18)$$

We see that the original energy-frequency relation on the particle frame results in a combination of energy-frequency and momentum-wave number relations.

From the 4-vector version of the special relativity, the Lorentz transformation invariant relations in those conjugated components of $(\mathbf{P}, E)$, $(\mathbf{x}, \text{t})$ or $(\mathbf{k}, w)$ can be expressed as the covariance of the self-product scalars of 4-vectors *($\mathbf{P}$,iE/c),($\mathbf{x}$,ict)* and *($\mathbf{k}$,iw/c)* respectively. For de Broglie's approach however, the energy-frequency and momentum-wave number relations can be regarded respectively as one component of

$$P_m \cdot dx_m = \mathbf{h}dj , \qquad (19)$$

where P_m represents the 4-momentum (**P**,*iE/c*), x_m the 4-spacetime (**x**,*ict*). The

17

quantum phase j , being a scalar product of the 4-momentum and the 4-spacetime, is therefore invariant under Lorentz transformation. In addition, based on the Lorentz coordinate transformation, de Broglie's argument designated the location of the traveling quantum particle as a fixed position and considered solely the energy-frequency relation as resulted from the phase change depending on a "proper time". First of all, we see that de Broglie pointed out a Lorentz invariant principle of quantum phase to project the 4-momentum from the 4-spacetime onto a proper time component with the energy-frequency relation. Secondly, we conceive that the number of periods of phase change observed from the position of de Broglie's quantum particle in fact corresponds to the number of periods of quantum wave passing through a certain position of observation.

This process reminds us that although the pure temporal RSJ flow was devised to describe a point Josephson junction, we may as well consider it a projected component of a spatial-temporal system, on condition that the driven Josephson oscillation resulted from a point measurement of two coupled waves propagating with the same velocity. In other words, both of the phases not only undergo temporal evolution at a fixed position, but also develop spatial variation at any instant.

As we know in the Josephson effect, this condition may be fulfilled by a line junction exposed to a magnetic field. If we assume the voltage drop across the Josephson junction plays exactly the role of the electric potential of a relativistic 4-potential, the Josephson energy-frequency relation can be traced back to an inner product of 4-vectors:

$$dj = \frac{qA_m \cdot dx_m}{h} \tag{20}$$

where A_m implies the electromagnetic 4-potential. From this assumption, we soon arrive at a conclusion that the Josephson oscillation can be regarded as a temporal

18

projection of a traveling Josephson wave which stands for the propagation of Josephson vortices, or magnetic fluxes, in which case the phase difference of the Josephson wave can be directly expressed as

$$dj = \frac{q}{\mathbf{h}}(\mathbf{A} \cdot d\mathbf{x} - Vdt) \tag{21}$$

where **A** represents the vector potential, **x** represents the space vector and *V* is the voltage drop across the Josephson line junction. It is interesting to notice that this spatial-temporal expression of the Josephson phase difference looks just like the Gauge Invariant phase difference, both play the role of a covariant variable in the spatial-temporal system. As we are considering the projection of 4-vectors, it is also of help to examine the orthogonal component, namely the space and momentum component. According to the two-phase coupling mechanism, we believe that a spatial-temporal quantization of the 4-momentum generalized from a temporal quantization of energy should find its quantized momentum component as we transform the 4-spacetime to its pure spatial component. For a propagating wave, a pure space-dependent state evolution at a frozen time can only be obtained from a snapshot covering the course of propagation. Thus as a same period of state evolution is concerned, the transformation from a time-dependent state evolution to a purely space-dependent pattern implies two fundamentally different recognizing processes of phase measurement. The process of the former implies a temporal counting at a specific position in linear space while the latter process implies an extended spatial recording at a fixed time. In addition, compared to the Lorentz transformation according to different observation points, we conclude for this temporal-to-spatial transformation that it is the absolute value of the phase, instead of its function forms of spatial-temporal dependence, are invariant.

For the driven Josephson system, we may as well apply the 4-vector scheme to

the driving field, on condition that it also bears a wave nature. Thus, we imagine $d\boldsymbol{j}$ in Josephson-RSJ flow as the phase change due to propagation of Josephson vortices and $d\boldsymbol{q}$ represents the phase change due to propagation of applied EM wave, both are covariant. The phase relation (7) can thus be written as an inner product of the 4-wave vector and the 4-spacetime:

$$d\boldsymbol{q} = k_{ml} \cdot dx_m, \tag{22}$$

where k_{ml} represents the 4-wave vector of the driving field. This phase-locking quantization approach also finds an inspiration from the fact that the frequency ratio of RSJ flow can actually be reduced to a simple phase ratio which is eventually independent either on time or on space. This implies that if there is a covariant relation describing the evolution of the phase ratio, we are free to transform the spatial-temporal description into a temporal phase-locking behavior that provides a simple dynamical mechanism for the rational quantization of energy and/or momentum.

From the ratio of (20) and (22), we may have

$$\frac{d\boldsymbol{j}}{d\boldsymbol{q}} = \frac{qA_m \cdot dx_m}{\mathbf{h}(k_{ml} \cdot dx_m)}, \tag{23}$$

which apparently is a Lorentz invariant scalar.

2-3　　Quantum Hall Effects and Quantum Phase-Locking Analogy

From the spatial-temporal to temporal projection conjecture described in section 2-2, we find this dynamical system a possible application to the Quantized Hall effects[8,9]. Since once we imagine the transverse Hall voltage V_H of a 1D composite flux channel as the voltage drop across a Josephson-like junction, and express the longitudinal Hall current as:

$$I_H = \frac{q}{2p}\frac{dq}{dt},$$ (24)

where q denotes the phase of the traveling electron wave, we can express the Hall resistance as

$$R_H = \frac{V_H}{I_H} = \frac{\dfrac{\mathbf{h}}{q}\dfrac{dj}{dt}}{\dfrac{q}{2p}\dfrac{dq}{dt}} = \frac{h}{e^2}\frac{dj}{dq}.$$ (25)

This relation applies not only to the small current single junction picture but also to the large current situation in which an array of parallel line Josephson-like channels is developed. The most noteworthy consequence of this argument would be that based on the rational phase locking mechanism, both quantized Hall effects, IQHE and FQHE, can be understood as resulted from a same dynamical mechanism.

　　An intuitive description for the macroscopic quantum vortex can be found in P.W. Anderson's consideration on the superfluid[10]. The Josephson oscillation was represented by a simple dynamical picture of phase slip. Fig. 2-1 (a) represents an isolated vortex. Any path circling around the vortex would experience a phase difference of $2p$. When a vortex travels from the left to the right as shown in Fig. 2-1 (b), there will be a phase difference of $2p$ developed across the barrier between the side 1 and side2.
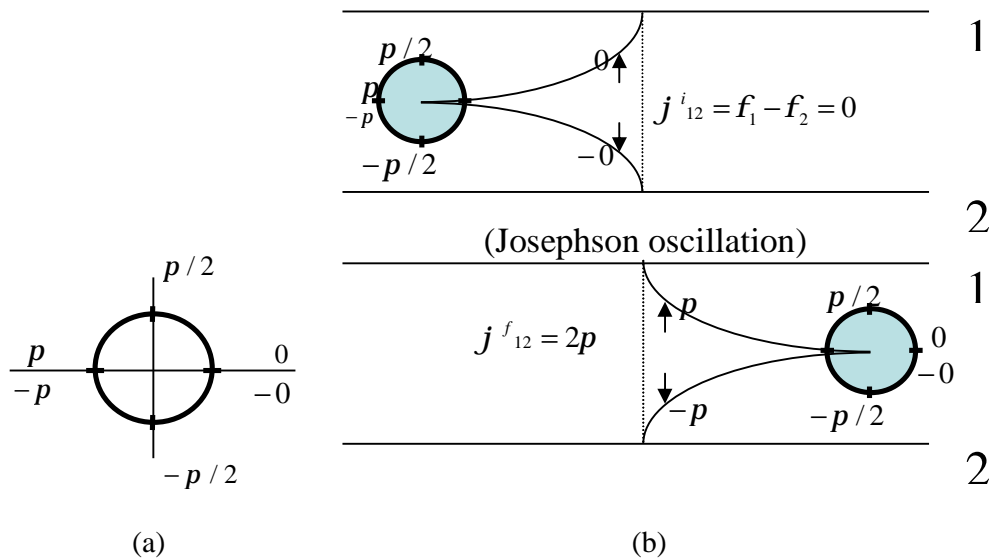
Fig. 2-1. (a) An isolated vortex. (b) Phase difference of $2p$ would be introduced to the two sides, side 1 and side 2, across the barrier when a Josephson vortex was traveling from the left to the right of a fixed observing position.

If we simply transform the observing position from the fixed coordinate to the vortex, we get the picture shown in Fig. 2-2. As the Hall current flows from the right of the flux to the left of the flux, a phase difference of $2p$ can also be measured between the side 1 and side 2 at a point reference point fixed with the flux. Combining with the phase change of the electronic wave this simple phase locking picture results in the quantized Hall effects, integer or fractional.

$$j^i_{12} = f_1 - f_2 = 0$$

$$j^f_{12} = 2p$$

(Hall Effect)
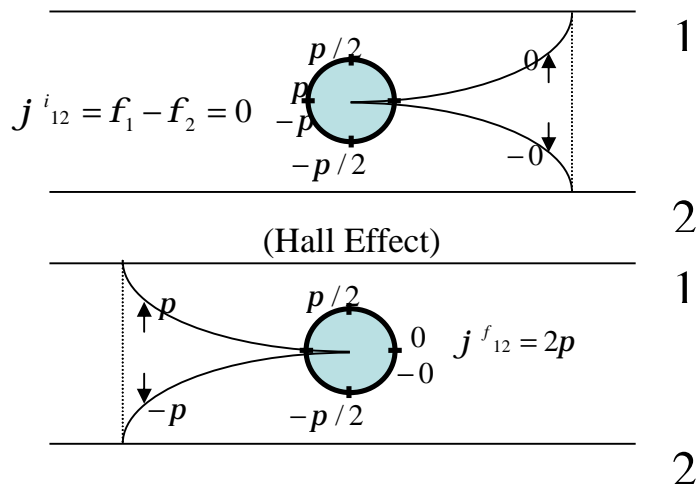
Fig. 2-2. Taking the observing coordinate of the flux, the Josephson oscillation of Fig.

2-1. can be transformed into quantum Hall system as the Hall electronic

wave from right to the left results in the phase difference across the current

strip between side 1 and side 2.
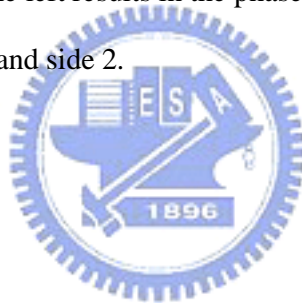
Although the Integer Quantum Hall effect and the Fractional Quantum Hall effect are usually considered as two different physics pictures, the former as a one particle system and the latter as a many particle interaction system, we still find some evidences suggesting a possible common Josephson coupling mechanism for quantum Hall effects.

The first kind of experiments implying the possible existence of dissipationless current channels with Josephson coupling can be found in the current induced breakdown of QHE[11]. The critical Hall current density was found to be proportional to the sample width as shown in Fig. 2-1. The bulk distribution of the Hall current from this sample width dependence supports the existence of parallel channels, which are essential for the inter-channel coupling with a voltage difference of

$V_H = \mathbf{h} w_H / q$.
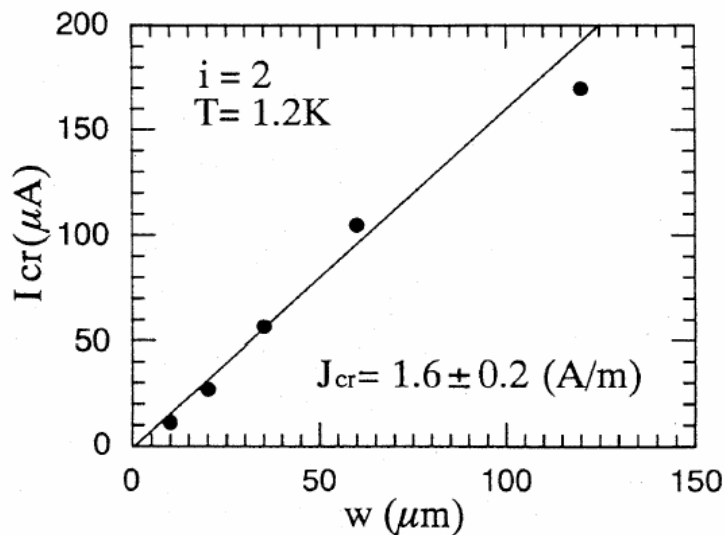
Fig. 2-3 Critical current versus sample width w for a wafer with a mobility of 2.1*10^5 cm2/Vs. The slope of the full line corresponds to a critical current density of 1.6A/m[12].

Actually it has been proposed that the current in the bulk flows in a manner of alternating sequence of compressible and incompressible strips[13]. It is reasonable to consider the incompressible Hall current strips play the role of condensed state with coherent quantum phase. And the compressible strips play the role of barrier across which a Josephson like voltage is developed.

Besides the possible Josephson coupling proposed here for the transverse voltage or the Hall voltage there are two other intriguing behaviors apparently related to the Josephson coupling. One is the longitudinal voltage behaviors during the current-induced breakdown, the other is the coherent coupling in bilayer quantum hall systems. The former system has been reported exhibiting typical nonlinear dynamical behaviors including hysteretic and chaotic time evolutions[14]. Among other models for the QHE breakdown, the work of D.J. Thouless et. al.[15], may shed some light on the coupling picture by assuming an abrupt formation of a metallic conduction path from one edge of the sample to the other. It is possible that fluxes are forced to move along this path and result in quantized longitudinal voltage. The latter bilayer quantum Hall system has been intensively investigated as a Josephson coupling system of two condensed n-p exciton layers[16]. As the distance between the two layers is comparable to that of two electrons within a layer, the Josephson like coherent tunneling appears between the two quantum Hall layers. It seems to the author that the boundary between the Josephson effect and the quantum Hall effect is becoming more and more difficult to define.

Summary

In this chapter we consider the Josephson voltage frequency relation as a de Broglie energy frequency relation and follow the relativistic derivation of momentum-wave number relation to find a spatial-temporal wave generalization for the driven Josephson oscillation. Focusing on the dissipative phase locking mechanism, a low dimensional nonlinear dynamical system was shown to be capable of connecting the driven Josephson ac effect and Quantized Hall effects. A macroscopic phase-locking quantization scenario is thus suggested to provide a simple common understanding for IQHE and FQHE.

References

[1] S. Shapiro, Phys. Rev. Lett., Vol. 11, 80 (1963).

[2] V.N. Belykh et. al., Phys. Rev. B. Vol. 16, 4860 (1978).

[3] W.C. Stewart, Appl. Phys. Lett., Vol. 12, No. 8, 277 (1968).

[4] D.E. McCumber, J. Appl. Phys., Vol. 39, No. 7, 3113 (1968).

[5] B.D. Josephson, Phys. Lett., Vol. 1, 251 (1962).

[6] For example, see D.G. McDonald, Science, Vol. 247, 177 (1990).

[7] For review, see L.de Broglie, "Non-linear wave mechanics a causal interpretation",
    English translation, Elsevier Publishing Company (1960).

[8] K. von Klitzing et. al., Phys. Rev. Lett., Vol. 45, No. 6, 494 (1980).

[9] D.C. Tsui, H.L. Stormer and A.C. Gossard, Phys. Rev. Lett., Vol. 48, 1559 (1982).

[10] P.W. Anderson, Rev. Mod. Phys. Vol. 38, 298 (1966).

[11] G. Nachtwei, Physica E, Vol. 4, 79 (1999).

[12] S. Kawaji, H. Hirakawa and M. Nagata, Physica B Vol. 184, 17 (1993).

[13] D.B. Chklovskii, B.I. Shklovskii and L.I. Glazman, Phys. Rev. B, Vol. 46, 4026
     (1992). D.B. Chklovskii, K.A. Matveev and B. Shklovskii, Phys. Rev. B, Vol. 47,
     12 605 (1993). K. Lier and R.R. Gerhardts, Phys. Rev. B Vol. 50, 7757 (1994).

[14] G. Boella, L. Cordiali, G. Marulloreedtz, D. Allasia, G. Rinaudo, M. Truccato
     and C. Villavecchia, Phys. Rev. B, Vol. 50, 7608 (1994).

[15] V. Tsemekhman, K. Tsemekhman, C. Wexler, J.H. Han and D.J. Thouless,
     Phys.Rev. B, Vol. 55, 10201 (1997).

[16] S.M. Girvin, Int. J. Mod. Phys. B, Vol. 17, 4975 (2003), M.M. Fogler and F. Wilczek,
     Phys. Rev. Lett. Vol. 86, 1833 (2001).

Chapter 3   RHEED Intensity Oscillation in Laser Ablation Epitaxy Growth

Another oscillation in two dimensional system to be investigated is the Reflection High Energy Electron Diffraction (RHEED) intensity oscillation in a laser ablation epitaxy[1-6]. During a properly controlled Epitaxial thin films growth, the periodic RHEED intensity oscillations have been proved to be as a direct mapping of layer-by-layer growth[7-10]. A period of RHEED oscillation corresponds to a cycle from (a) to (e) of monolayer Epitaxial growth as schematically shown in Fig. 3-1[6].

(a)   (b)
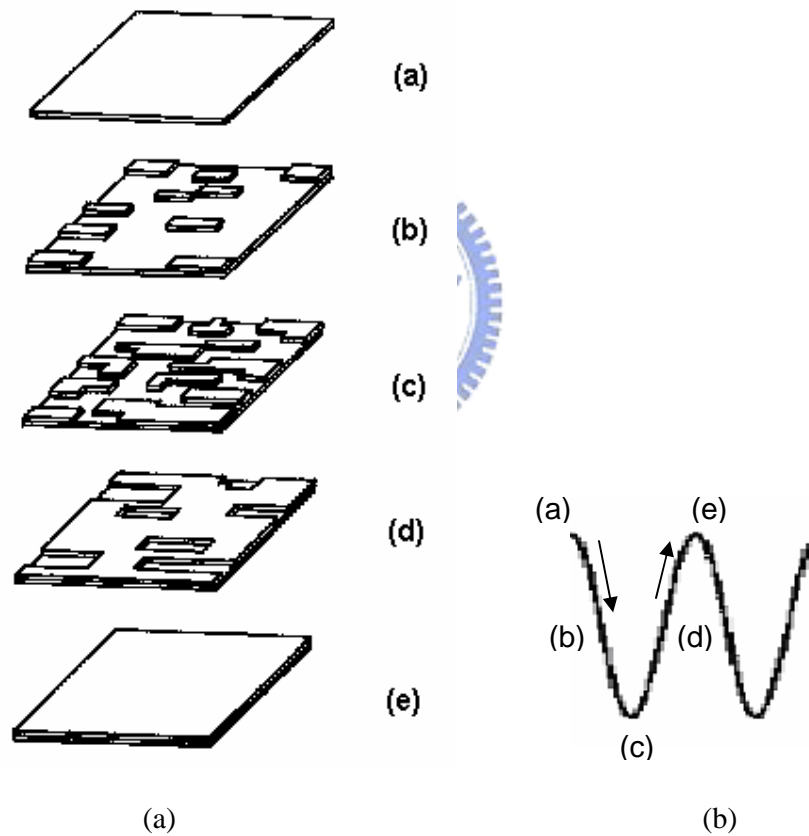
Fig. 3-1. (a) An idealized monolayer growth corresponding to a period of RHEED oscillation. (b) The RHEED intensity oscillation corresponding to a cycle of monolayer growth.

3-1   RHEED-Reflection High Energy Electron Diffraction

Although RHEED intensity monitoring has long been used to monitor Epitaxy growth[1-6], Fig. 3-2., a quantitative modeling of the recorded intensities remains open due to the multiple (dynamical) scattering caused by strong interaction of electrons with the surface.
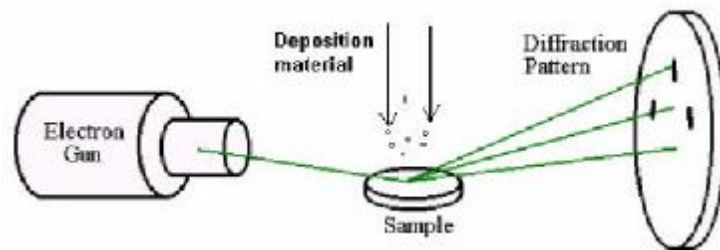
Fig. 3-2. Schematics of the RHEED monitored thin film growth.

Dynamical calculations of RHEED intensities require long computation times even when oversimplified assumptions about incomplete layers are made[11]. The surface morphology, for example, island shapes, is not treated dynamically. On the other hand, the single-scattering picture of kinematical approximation directly relates surface structure and scattered intensity[12,13]. To be noted that the relation of the kinematically calculated intensities to real RHEED data often appears questionable.

Geometric theory appears to be the simplest theory to describe RHEED. Diffraction of a plane wave with wave vector k by a single crystal is assumed and no interaction mechanism is involved. Diffraction happens when the Laue condition is satisfied:

$$k'-k_0 = G,\qquad\qquad\qquad\qquad\qquad (1)$$

where k' and k_0 are the wave vectors for the diffracted and the incident beams respectively and G is the reciprocal-lattice vector. In the case of elastic scattering, $|k'| = |k_0|$. Infinite numbers of k' vectors pointing in all directions form the so-called Ewald sphere. Ewald sphere is a sphere that has its origin as the origin of the k_0 and a radius $|k_0|$. The Laue condition is "diffraction occurs for all $|k_0|$ connecting the origin of the sphere and a reciprocal-lattice point". The magnitude of the wave vector is given by the relativistic expression

$$k_0 = \frac{2p}{l} = \frac{1}{\mathbf{h}}\sqrt{2m_0qV + (\frac{qV}{c})^2} \tag{2}$$

where m_0 is the electron rest mass, q is its charge and V is the accelerating potential. Expression (2) can also be written as

$$l = \frac{h}{\sqrt{2m_0qV + (\frac{qV}{c})^2}} \approx \frac{12.3}{\sqrt{V(1 + 1.95\times10^{-6}V)}}, \tag{3}$$

where l is measured in Å and V in volts.

The kinematic theory is straightforward for understanding of RHEED, however no description of the diffraction mechanisms is provided. A more advanced theory treated quantum-mechanically the interaction between the incident wave and the scatterer by solving the Schrödinger equation for the wave function of the scattered wave, $y(\underline{r})$, given an effective potential $U(\underline{r})$;

$$(\nabla^2 + U(\underline{r}) + k_0^2)\Psi(\underline{r}) = 0. \tag{4}$$

By introducing Green's method, equation (4) could be reformed into

$$y(\underline{r}) = e^{i\underline{k}_0 \cdot \underline{r}} - \frac{1}{4p} \int \frac{e^{ik|\underline{r}-\underline{r}'|}}{|\underline{r}-\underline{r}'|} U(\underline{r}')y(\underline{r}')d\underline{r}'. \qquad (5)$$

The first term represents the incident plane wave, the second term represents the

scattered wave. From the point of view of experiments, one is more concerned with

$y(\underline{r})$ with large distances compared to the dimension of the scatterers $|\underline{r}-\underline{r}'| \sim r$. In

this situation, equation (5) is further refined as

$$y(\underline{r}) = e^{i\underline{k}_0 \cdot \underline{r}} - \frac{e^{ik'r}}{4pr} \int e^{-i\underline{k}' \cdot \underline{r}'} U(\underline{r}')y(\underline{r}')d\underline{r}'. \qquad (6)$$

The part of the second term

$$f(\underline{k}) = -\frac{1}{4pr} \int e^{-i\underline{k}' \cdot \underline{r}'} U(\underline{r}')y(\underline{r}')d\underline{r}' \qquad (7)$$

is the scattering amplitude.

The current scattered into a solid angle $d\Omega$ per unit current density in the incident

wave is given by

$$I(q,f)d\Omega = |f(q,f)|d\Omega. \qquad (8)$$

Kinematic theory evolves as the Born approximation is adopted. The wave

function in the crystal is assumed to be the same as the incident wave or $y(r') = e^{ik_0 r'}$.

In this case, equation (7) is rewritten as

$$f(\underline{K}) = -\frac{1}{4p} \int e^{-i\underline{K} \cdot r'} U(\underline{r}')d\underline{r}', \qquad (9)$$

where $\underline{K} = \underline{k}' - \underline{k}_0$. The scattering amplitude is defined as the Fourier transformation of

the scattering potential. Calculations have been made for the scattering amplitude by

31

PDF created with FinePrint pdfFactory trial version http://www.fineprint.com

functional forms for $U(r)$ with the periodicity of the crystal lattice. Compared to dynamic approach, the kinematical treatment oversimplifies the diffraction by assuming that the wave function at the scatterer equals that of the incident plane wave. This assumption overlooks the mutual interaction between the crystal and the incident electron beam.

The dynamical theory is introduced to deal with the diffraction problem without the oversimplification of the kinematical theory. For electron scattering in a crystal, the wave within the crystal may be represented by a sum of plane waves

$$y(r') = \sum_{l=0}^{N} y_l(r') e^{ik_l \cdot r'}. \tag{10}$$

Substituting (10) into (7) and using the Laue condition, $k_l - k_0 = 2pl$, the scattering amplitude can be written as

$$f(k) = \sum_{l=0}^{N} f_l(K_l) = -\frac{1}{4p} \sum_{l=0}^{N} \int_{scatterer} y_l(r') e^{-i(k'-k_0-2pl)\cdot r'} U(r') dr'. \tag{11}$$

To find the scattering amplitude, the integrals in equation (11) have to be solved. And the difficulty embedded in the integration often increases the complexity of the dynamical theory analyzing RHEED data.

Starting from the Schrödinger equation:

$$(\nabla^2 + U(r) + k_0{}^2) y(r) = 0,$$

where k_0 is the incident wave vector and the scaled lattice potential $U(r)$ equals $\frac{2me}{\mathbf{h}^2} V(r)$, we consider only the elastic scattering for $|k_0| = |k'|$, where k' is the scattered wave vector. The RHEED diffraction can be demonstrated as Fig. 3-3. For RHEED the Ewald sphere is large. For 20 keV the incident vector is 785 /nm, about

70 times of the reciprocal lattice unit of GaAs. The large radius of the Ewald sphere

with the grazing angle justify the small angle approximation.
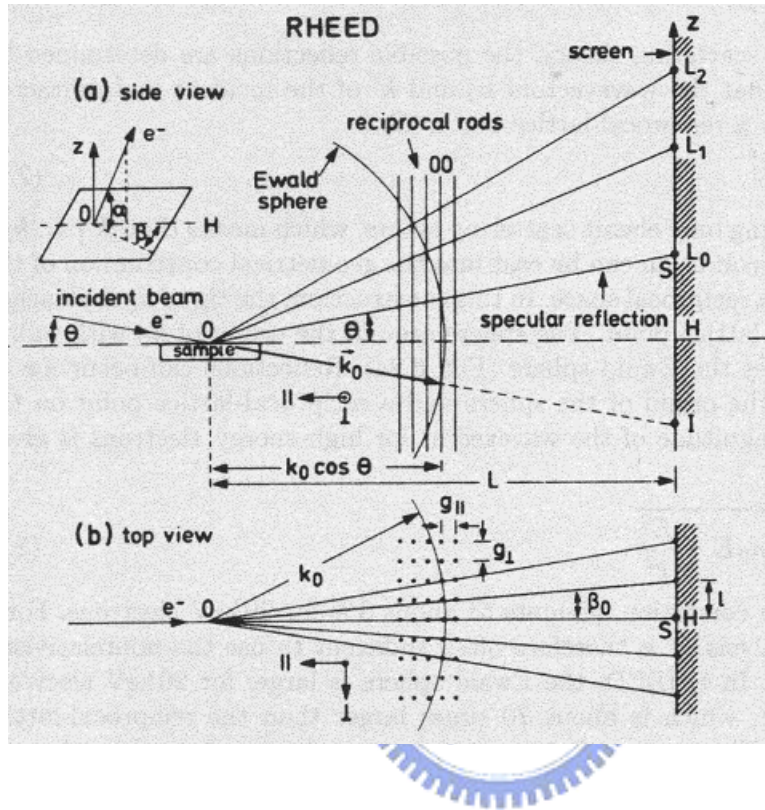
Fig. 3-3. Ewald sphere construction and diffraction geometry of RHEED.

Intensity maxima correspond to intersections of the Ewald sphere and the reciprocal

lattice.

To get an estimated scattering cross-section, one considers the potential of a

single atom with Thomas-Fermi screening:

$$V(r) = \frac{Ze^2}{4pe_0 r}\exp(-\frac{r}{a}),\tag{12}$$

where the screening length a is defined as $\dfrac{4pe_0 \mathbf{h}^2}{me^2 \sqrt[3]{Z}}$ with Z, the atomic number of

the atom and e_0, the vacuum permittivity. For the Born approximation the total

cross-section will be

$$s = \frac{16pm^2e^4}{\mathbf{h}^4(4pe_0)^2}\frac{Z^2a^4}{4k^2a^2+1}.$$ (13)

From estimation of real cases, the cross section area is too small for the kinematic theories to fully account for the diffraction. Multiple scattering is highly possible in all cases. On the other hand, due to the simplicity of the kinematical treatments, single scattering is still the main consideration in modeling RHEED diffraction.

A typical diffraction pattern consists of Bragg reflection spots, streaks, Kikuchi lines as well as shadow edges. The Bragg reflection spots can be constructed by intersecting Ewald sphere with the radius of incident wave vector and the reciprocal lattice rods. These spots lie on an arc known as the Laue zone. Streaks are formed by the momentum distribution of electrons, instrumental reasons and surface morphology. For disordered surfaces the lateral disorder is associated with a broadening of the reciprocal lattice rods. Kikuchi lines resulted from the diffraction of electrons which have been scattered during entering the solid. In the k space, the reciprocal lattices of a 3D crystal form a group of dots. Due to the nature of a perfect 2D plane, the reciprocal lattices become rods as shown in Fig. 3-4.
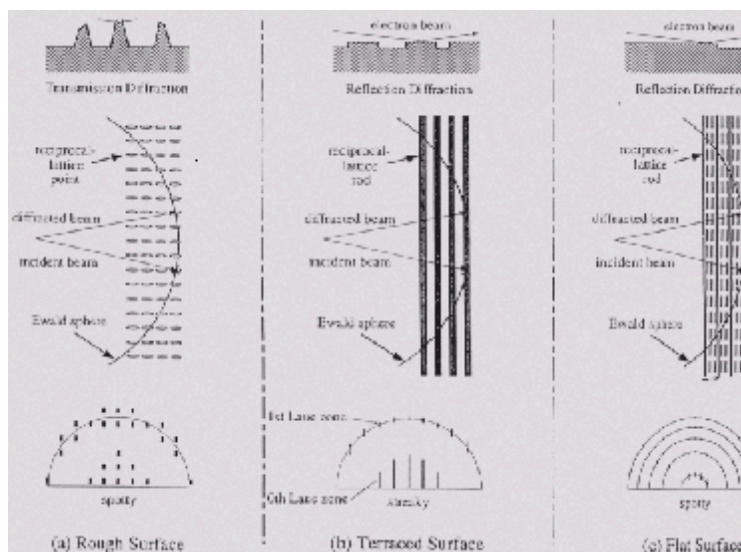
Fig. 3-4. RHEED diffraction on surfaces with different flatness.

34

　　　　Our laser depositing system consists of a KrF excimer laser with a pulse duration

of 30 ns operating mainly at the repetition rate range of 1-5 Hz. The target was a

single crystalline disk of SrTiO3. The typical energy density was 2 Joule/cm2.

STO(100) substrates were attached to a plate stage with resistive heating coil. The

films were deposited at various temperatures by adjusting the current applied to the

resistive heating block under the oxygen partial pressure of 5×10^{-4} Torr. The

system schematics is as shown in Fig. 3-5.
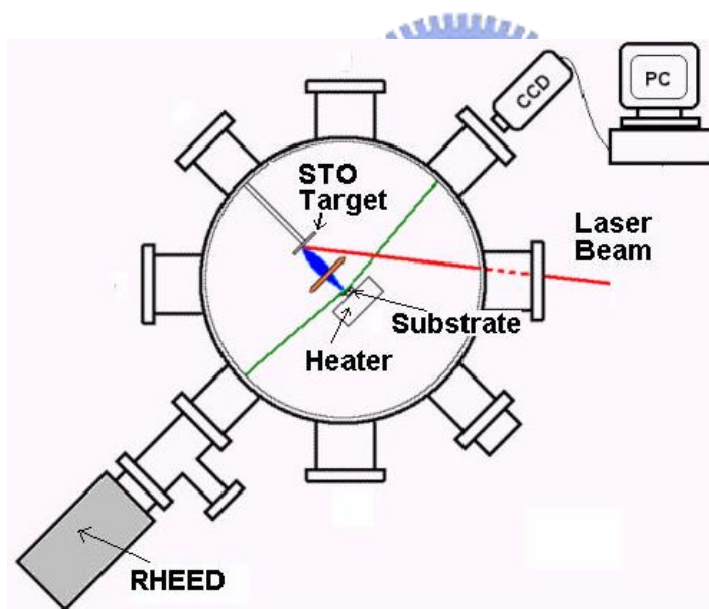
Fig. 3-5. RHEED in-situ monitored pause laser deposition system.

　　　　During the deposition or anneal processes, the intensity of the RHEED specular

beam was monitored by RHEED. A 20 keV electron beam was ejected along the

surface of STO substrate with a grazing angle of 0.7 degree. With a de Broglie

wavelength of about 0.86 Å, the grazing electron beam is slightly off-Bragg condition

and the RHEED intensity is expected to be most sensitive to the step edges on the surface[6].

Fig. 3-6 shows a group of oscillations of the RHEED specular reflections as a function of temperature for the homoepitaxial STO films grown on stepped substrates[14].
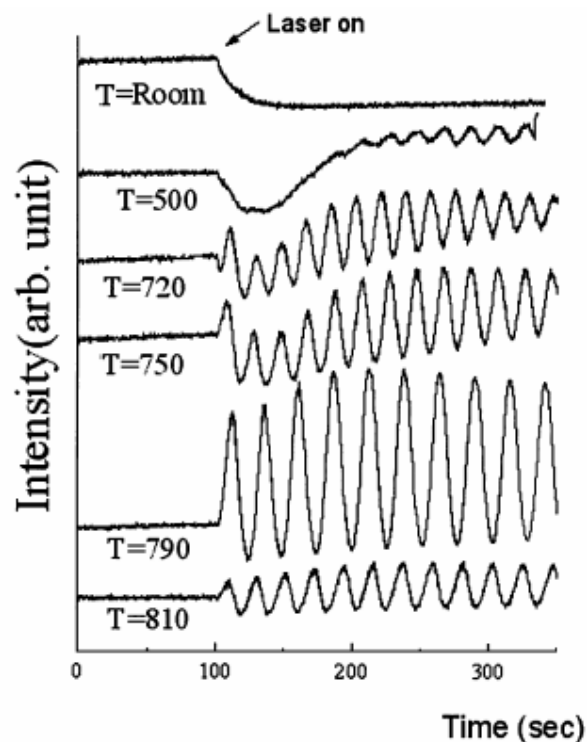
Fig. 3-6. RHEED oscillation for STO deposition on stepped substrates.

One notices in Fig. 3-6 the amplitude and periodicity of the oscillations change with the deposition temperature. Since, in all cases the repetition rate (1 Hz) and energy density (2 J/cm2) of the laser were kept unchanged, the amount of material contained in the plume of every laser pulse should be approximately the same. As a result, a fixed oscillation periodicity is expected for a strict layer-by-layer growth.

Alternatively, the undamped RHEED oscillations can occur as a result of changing step density distribution, while damping results from increasing contribution of third level[15,16].

In this scenario, the lack of oscillation at low temperatures can be understood as a consequence of low diffusivity. It not only hinders the coalescence between nuclei but also distributes steps over multiple layers. At higher temperatures, the enhanced diffusivity helps the redistribution of the surface steps, leading to the oscillatory behavior of RHEED intensity. This explains the temperature dependence of the emergence as well as the amplitude and periodicity of the RHEED intensity oscillations observed.

3-3   RHEED Intensity Oscillation and Step Edge Evolution of Epitaxy Deposition

   and Diffusion Competition

   The RHEED intensity oscillation can be deemed as resulted from a competition

between the source material adsorption and surface diffusion. For a substrate with

step structure, this competition scenario has been reported to provide a method to

extract valuable kinetic information from the RHEED intensity[17].
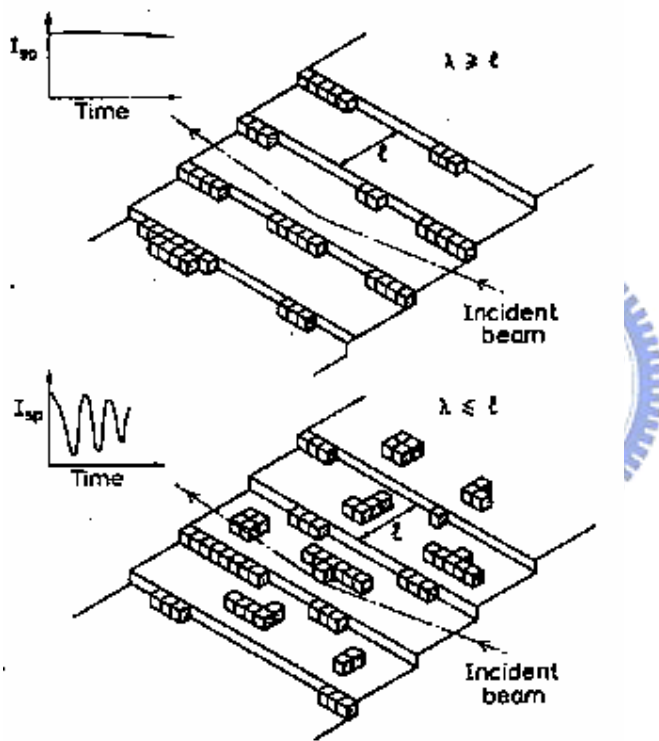
Fig. 3-7. Competition between deposition and diffusion in RHEED intensity

oscillation of the Epitaxy growth of a stepped film[17].

When the deposition adsorption is faster than the diffusion of adatoms, the diffusion

length l will be less than the step distance l and there will be oscillation in the

RHEED intensity, as shown in the lower part of Fig. 3-7. On the other hand, if the

diffusion rate is increased as in the higher temperature condition, the adatoms have

enough time to move to step edges and the growth appears as a step flow mode with the RHEED intensity kept unchanged as shown in the upper figure.

This temperature dependence of the competition has been used to determine the diffusion length as 590°C shown in Fig. 3-8.
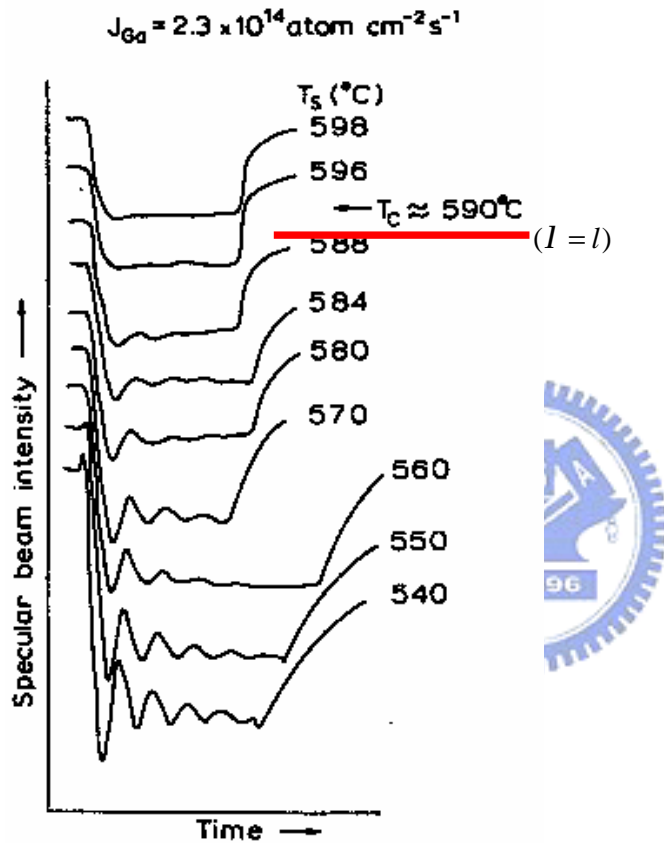
Fig. 3-8. RHEED intensity oscillation appears when the epitaxy growth changes from the step flow mode to layer-by-layer mode as the temperature decrease. A threshold temperature can be obtained to determine the diffusion length for the stepped substrate.

Further from the dependence of the threshold temperature on the deposition rate, Neave et. al. obtained the diffusion coefficient and the activation energy of the

39

Epitaxial growth.

To investigate the competing deposition and diffusion of the layer by layer growth as well as the RHEED oscillation, a series of RHEED intensity monitored deposition and annealing have been conducted separately on STO films. Before introducing the results of the diffusion kinetics, we review first an important result of the laser deposition of STO films monitored by RHEED.

Although the application of RHEED in Epitaxy growth has been shown successful, the detailed diffraction mechanism has yet to be concluded. In principle the higher intensity represents a smoother plane and the low intensity represents a rougher surface, there are still two theories under debate. According to a two layer interference picture, the topmost surface coverage can be equalized to the RHEED intensity[18]. Another diffraction mechanism related reciprocally the RHEED intensity to the step edge density[19]. From the evidences currently available, neither theory can claim to be a complete solution for all the material conditions. For example, the step edge density theory encountered challenge in the high density regime in which the RHEED intensity even evolves proportional to the edge density[20,21].

During the study of RHEED oscillation, a series of the RHEED monitored interrupted laser deposition for the SrTiO3 film growth was conducted[22,23]. An evident result differentiating these two pictures was observed in a series of deposition and annealing experiments.

The as-polished STO sample was deposited by laser ablation with various repetition rate but same account of pulses during which the RHEED intensity oscillates to show layer growth. The RHEED intensity experienced a sudden drop each time the laser was turned on again after the same amount of deposition was interrupted and the sample was annealed for a same period of time. As shown in Fig. 3-9.
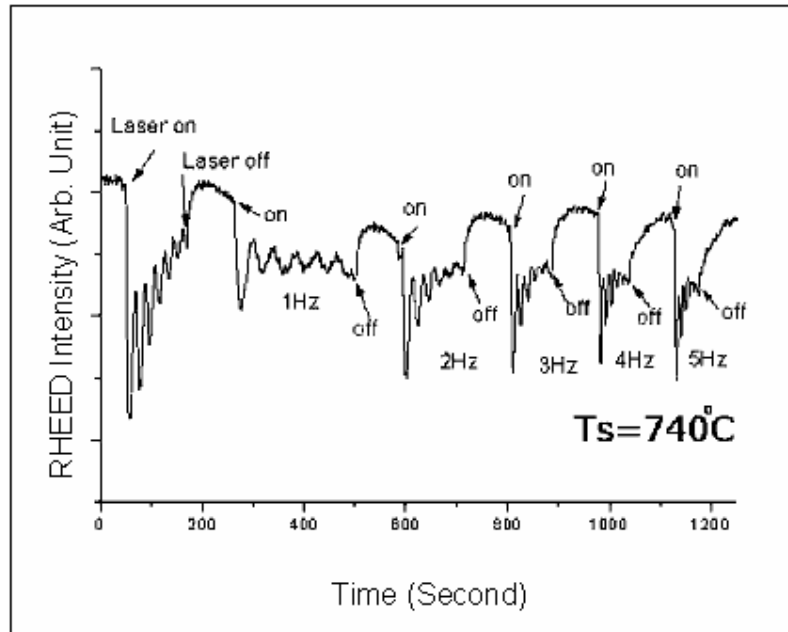
40

Fig. 3-9. A series of deposition-annealing RHEED monitoring was conducted for the laser repetition rates from 1 Hz to 5 Hz. The deposited amounts of STO were estimated the same for each sudden drop at all the laser turn-on points with 14~17 pulses respectively.

Since the laser account was measured to be 14 to 17 for the RHEED intensity drops for all repetition rates from 1Hz to 5 Hz, the amount of materials deposited or the coverage of the surface should be approximately the same. However from the RHEED intensity drop data as shown in Fig. 3-10, the drop depth was proportional to the repetition rate.

41
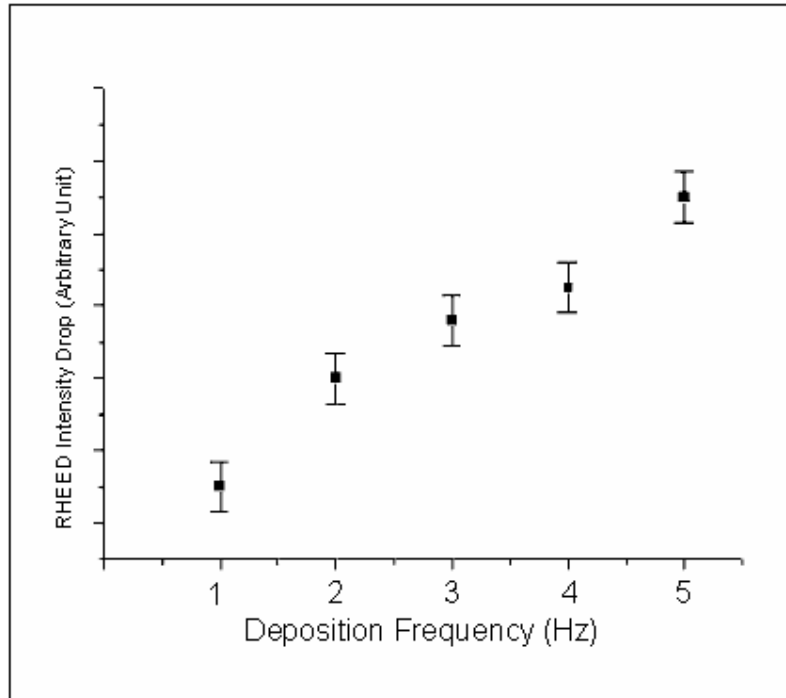
Fig. 3-10. The RHEED intensity drops in Fig. 3-9. were found to increase with the increased laser repetition rate, suggesting step edge density accounts for the RHEED diffraction instead of topmost layer coverage which was kept unchanged for all 5 repetition rate by the same total pulses.

This proportionality implies that as the step edge density was increased by increasing the deposition rate as well as the number of islands formed under the assumption of monolayer deposition [24,25], the RHEED intensity dropped more. Therefore the density of one dimensional step edges, namely the edge dislocations or the screw dislocations, can be regarded as the key variable revealed by the RHEED intensity.

42

References

[1] "Applied Rheed: Reflection High-Energy Electron Diffraction During Crystal Growth", Braun, Wolfgang, Springer-Verlag Berlin and Heidelberg GmbH & Co. KG, 1999.

[2] "Reflection High-Energy Electron Diffraction and Reflection Electron Imaging of Surfaces", Edited by P. K. Larson and P. J. Dobson, Plenum Press New York and London, 1988

[3] J.J. Harris, B.A. Joyce, P.J. Dobson, Surf. Sci. 103, L90 (1981).

[4] C.E.C. Wood, Surf. Sci. 108, L441 (1981).

[5] J.M. van Hove, C.S. Lent, P.R. Pukite, P.I. Cohen and J. Vac, Sci. Technol. B 1 (1983) 741.

[6] J.H. Neave, B.A. Joyce, P.J. Dobson, N. Norton, Appl. Phys. A 31, 1 (1983).

[7] G. Koster et al., Appl. Phys. Lett. 73, 2920 (1998).

[8] M. Naito et al., Physica C 305, 233 (1998).

[9] D.W. Kim et al., Physica C 313, 246 (1999).

[10] T. Terashima et al., Phys. Rev. Lett. 65, 2684 (1990).

[11] P.A. Maksym, U. Korte, J.M. McCoy, H.J. Gotsis, Surf. Rev. Lett. 5, 873 (1998).

[12] C.S. Lent, P.I. Cohen, Surf. Sci. 139, 121 (1984).

[13] P.R. Pukite, C.S. Lent, P.I. Cohen, Surf. Sci. 161, 39 (1985).

[14] J. Y. Lee *et al.*, Physica B **284-288**, 2099 (2000).

[15] T. Frey et al., Phys. Rev. B 49, 3483 (1994).

[16] S. Stoyanov, M. Michailov, Surf. Sci. 202, 109 (1988).

[17] J.H. Neave, P.J. Dobson, B.A. Joyce and Jing Zhang, Appl. Phys. Lett. 47, 100 (1985).

[18] C. S. Lent and P. I. Cohen, Surf. Sci. **139**, 121 (1985).

[19] J. H. Neave, B.A. Joyce, P.J. Dobson and N. Norton: Appl. Phys. **A 31** (1983); S.

Stoyanov: Surface Sci. **199**, 226 (1988).

[20] U. Korte and P. A. Maksym, Phys. Rev. Lett. **78**, 2381 (1997).

[21] Z. Mitura, S. L. Dudarev and M. J. Whelan, Phys. Rev. B. **57**, 6309 (1998).

[22] J.Y.Lee, J.Y. Juang, K.H.Wu, T.M. Uen and Y.S.Guo: Surface Sci. **488** (3), 277 (2001).

[23] J.Y. Lee, T.C. Wang, S.F. Chen, J.Y. Juang, J.Y. Lin, K.H. Wu, T.M. Uen and Y.S. Gou: Chinese Journal of Physics **39** (4), L299 (2001).

[24] J. Y. Lee et al., Physica **B 284-288**, 2099 (2000).

[25] S. Stoyanov and M. Michai1ov, Surf. Sci. **202**, 109 (1988).

Chapter 4   RHEED Intensity Recovery and Activated Step Edge Diffusion

RHEED has been proved to be one of the most valuable tools to monitor and control the Epitaxy thin film growth[1-3]. During the layer by layer growth, RHEED intensity was found to oscillate with a period synchronized to the number of growing layers[2].

In the previous chapter we introduced the deposition and diffusion competition picture for layer by layer growth with the oscillating RHEED intensity. We also reviewed the dislocation density interpretation of RHEED intensity obtained from the results of RHEED monitored laser deposition, which results in the decreasing intensity of a RHEED oscillation. In this chapter we report the analyses on the RHEED intensity evolutions in annealing experiments for the diffusion characteristics which contributes to the surface smoothening and the increasing intensity in the RHEED intensity.
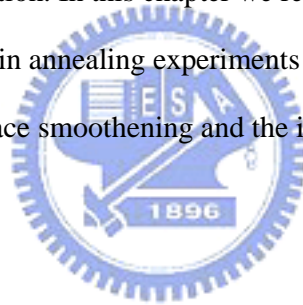
4-1   Thermally activated kinetics--Arrhenius plot and Kissinger plot

During the analysis of the diffusion characteristics in annealing experiments, we obtained two activation energies from the RHEED data by utilizing two kinetic methods. One is the Arrhenius method of isothermal annealing, the other is the Kissinger method of constant heating rate annealing. Both approaches can provide the activation energy through a logarithmic plot with respect to temperature. We review these two kinetic methods first.

The Arrhenius law states that at temperature T the molecules have energies according to a Boltzmann distribution, one expects the proportion of collisions with energy greater than E_b to vary with $\exp(-\dfrac{E_b}{k_B T})$. In terms of chemical reaction, the Arrhenius equation can be expressed as

$$k = ne^{-\frac{E_b}{k_B T}},$$ (1)

where k is defined as the rate constant, n is a pre-factor sometimes called the escape frequency. This relation can be derived from a transition state theory as follows[4].

The transition state theory can be regarded as a near-equilibrium theory of non-equilibrium behavior. The first assumption of the theory is the low temperature criterion: $E_b \gg k_B T$. For example, at the temperature region of 1000K, the activation barrier should be much larger than 0.1 eV. This criterion keeps the escaped particles as a small portion of the system such that the distribution function of the system differs little from the equilibrium Maxwell Boltzmann distribution. The second assumption is that the thermodynamic equilibrium is applicable to both the reactants and the activated species. The third assumption is the so-called

Non-recrossing assumption. Barrier crossing is assumed as an irreversible one way process.

For a N particle system, the partition function of a single particle can be expressed as

$$Z = \frac{1}{h} \int_{-\infty}^{\infty} \int_{-\infty}^{\infty} \exp[-bp^2/(2m) - bf(x)] dp dx \qquad (2)$$

where m is the mass, $f(x)$ is the potential. The classical distribution function is given by

$$f(p,x) = \frac{N}{hZ} \exp[-bp^2/(2m) - bf(x)] \qquad (3)$$

and $f(p,x)$ satisfies the normalization condition

$$\int_{-\infty}^{\infty} \int_{-\infty}^{\infty} f(p,x) dp dx = N. \qquad (4)$$

The particle flux crossing the barrier is given by

$$j = \int_{0}^{\infty} (\frac{p}{m}) f(p,0) dp. \qquad (5)$$

No-recrossing has been assumed by restricting the momentum integral to positive, the top of the barrier locates at x=0 and the distribution function at x=0 is

$$f(p,0) = (N/hZ) \exp[-bE_b - bp^2/(2m)]. \qquad (6)$$

The flux integral turns out to be

$$j = \frac{N}{hZb} \exp(-bE_b). \qquad (7)$$

Finally we have the rate constant of the transition state theory:

$$k_{TST} = \tfrac{j}{N} = n \exp(-\frac{E_b}{k_B T}), \qquad (8)$$

where the "escape frequency" $n = \dfrac{1}{hZb}$ and $\dfrac{1}{k_B T} = b$.

Transition state theory is somehow based on contradictory assumptions. The equilibrium should not be valid everywhere owing to the velocity symmetry of the Maxwell-Boltzmann distribution. Therefore no net flux should be found anywhere.

TST is better thought of a limiting case of some more logical theories such as Kramers theory[5], which can be derived from a Fokker-Planck type theory of Brownian motion. Starting from the distribution function evolution of Klein-Kramers equation:

$$\frac{\partial f}{\partial t} = -\frac{p}{m}\frac{\partial f}{\partial x} + g'\frac{\partial(pf)}{\partial p} + \frac{\partial}{\partial p}(f\frac{\partial f}{\partial x}) + \frac{\partial f}{\partial x}\frac{\partial f}{\partial p} + mg'k_BT\frac{\partial^2 f}{\partial p^2} \tag{9}$$

where $g' \equiv g/m$ and g represents the friction coefficient related to the diffusion coefficient D by the Einstein relation

$$D = k_BT/g, \tag{10}$$

the Kramers theory at high damping limit arrived at an Arrhenius type rate constant of

$$k_{Kh} = n\exp(-\frac{E_b}{k_BT}), \tag{11}$$

where the escape frequency is given by a combination of system parameters

$$n = \frac{1}{g'}\frac{w_0 w_b}{2p}.$$
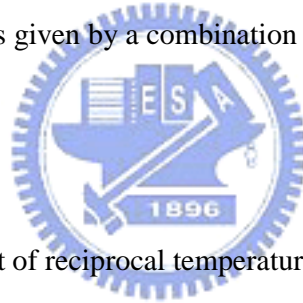
Another logarithmic plot of reciprocal temperature to obtain the activation energy is the Kissinger method[6]. The Kissinger equation can be expressed as

$$A\frac{a}{T_p^2} = \exp(-\frac{E_b}{k_BT_p}), \tag{12}$$

where a is the heating rate, T_p is the peak temperatures of differential enthalpy curves of different heating rates, E_b is the activation energy and A is a constant. By linearly fitting $\ln(\frac{a}{T_p^2})$ versus $1/T_p$ points for all differential enthalpy curves of different heating rates, the activation energy can be obtained from the slop of the logarithmic line. It was shown by Kissinger that for a reaction of the order n, the reaction rate being given by

$$\frac{dx}{dt} = A(1-x)^n \exp(-\frac{E_b}{k_BT}), \tag{13}$$

48

the reaction rate comes to a maximum during the constant rising of the temperature. Taking the time derivative of reaction rate equation (13) to be zero, one obtains the Kissinger equation (12). This equation has be generalized to solid state nucleation and growth reaction as well as the grain growth reaction[7], like the Arrhenius method. For a pure grain growth problem, the rate constant can be shown as

$$k = \frac{n}{T} \exp(-\frac{E_b}{k_B T}) \tag{14}$$

or sometimes expressed as a simple Arrhenius type form with negligible incorrectness

$$k = n \exp(-\frac{E_b}{k_B T}). \tag{15}$$

For the case in (14), it was shown that the Kissinger equation (12) should be rewritten as

$$A\frac{a}{T_p} = \exp(-\frac{E_b}{k_B T_p}). \tag{16}$$

From calculation of experiment data however, the activation energies obtained from (12) or (16) differs not much.

The dislocation density picture of RHEED intensity provides not only a geometric measure of the surface morphology but also kinetic information such as diffusion characteristics. In our investigation on the in-situ RHEED monitoring the interrupted deposition recovery, we found that the deposition-interrupted time-annealing curves possess temperature dependent features. As shown in Fig. 4-1, for the interrupted RHEED oscillation, the annealing data in insets showed clear temperature dependence as enlarged in Fig. 4-2.
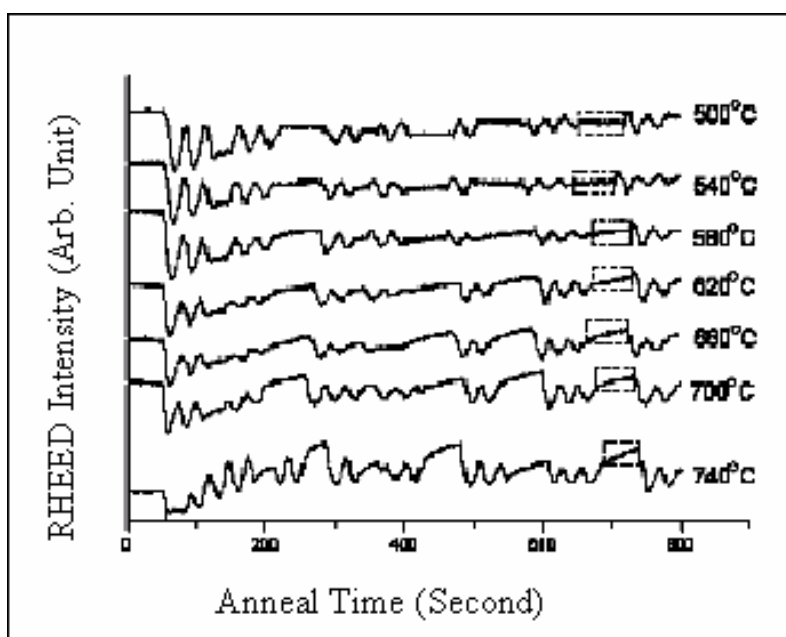
Fig. 4-1. Time evolution of RHEED intensity from 500°Cto 740C. Layer by layer growth can be confirmed from the oscillation for all curves. The insets show recovery from near peak positions of oscillations.
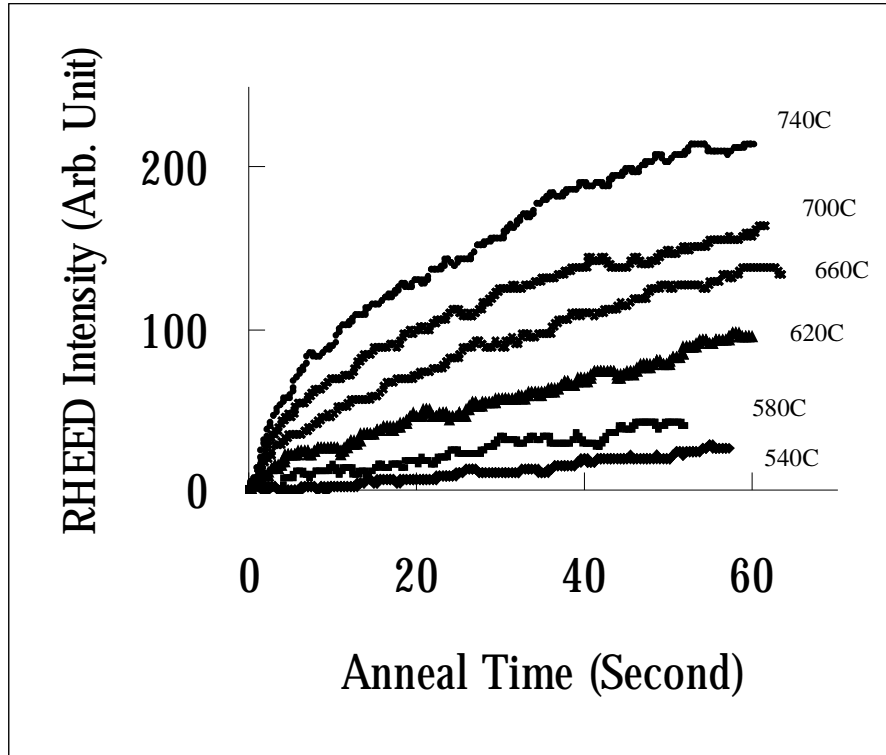
Fig. 4-2. Enlarged time curves of RHEED intensity during the annealing after the interrupted depositions in Fig. 4-1. The curvatures show a monotonic increasing dependence on temperature.

The most intriguing fact is the monotonic temperature dependence of the curvatures. Double-logarithmic plot were checked for these curves as shown in Fig. 4-3.
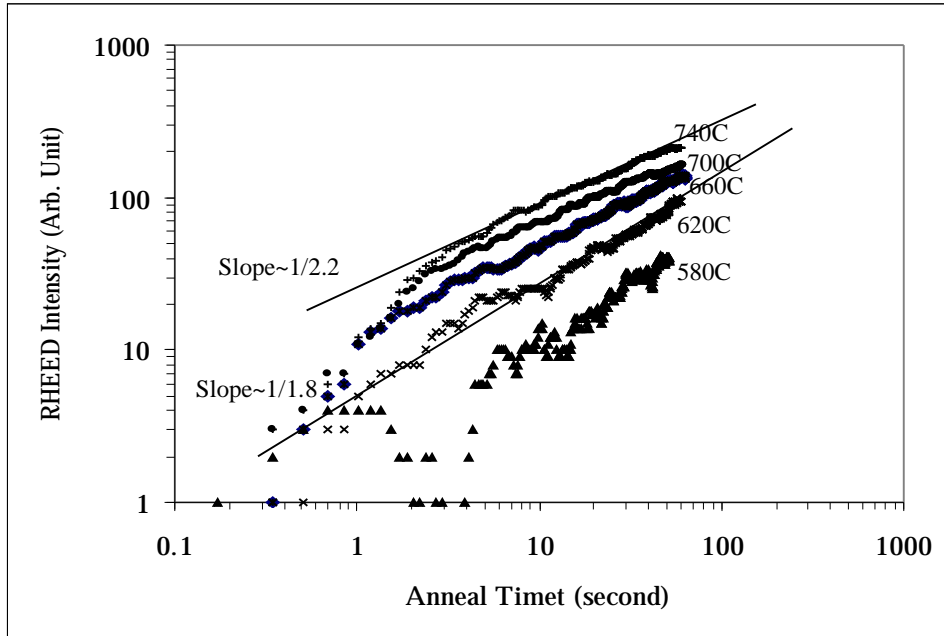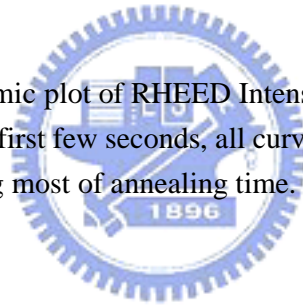
Fig. 4-3. Double logarithmic plot of RHEED Intensity vs. anneal time for various temperatures. Except the first few seconds, all curves display clear linearity with a slope of 2 +/- 0.2 during most of annealing time.

From the apparent linearity observed in these curves, one finds certain power law embedded in the time annealing RHEED intensity. Although in earlier papers[8] the temporal behavior of the annealing recovery curves were analyzed by exponential functions with corresponding time constants, it turns out that power law especially quadratic power time dependence as fitted in Fig. 4-4 may provide even straightforward kinetic information for the interpretation of RHEED intensity.
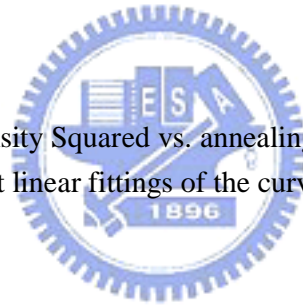
52
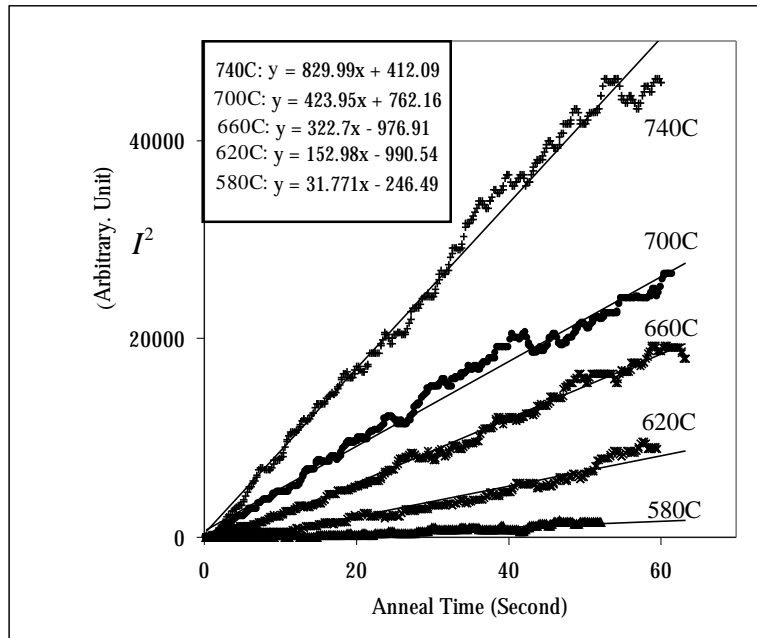
Fig. 4-4. RHEED Intensity Squared vs. annealing time for various temperatures. The inset shows perfect linear fittings of the curves. A monotonic dependence can be clearly seen.

In a RHEED intensity analysis of GaAs Epitaxy growth, Neave et. al.[9] developed a method for deciding the diffusion properties from the Einstein relation:

$$< x^2 >= 4Dt \tag{17}$$

where $< x^2 >$ represents the mean square displacement of adatom diffusion with the hopping time t and the diffusion coefficient D. The displacement was determined by the step separation of the substrate at temperature threshold between the step flow growth and the layer by layer growth. Diffusion time was calculated from the deposition rate. The activation energy was obtained from the Arrhenius plot by taking the temperature thresholds for various deposition rate. In such a kinetic study, the

53

RHEED intensity provided an indirect criterion to determine transition temperature of two different growth modes.

In our film annealing research, the time evolution of RHEED intensity was found to show quantitative dependence relation on temperature. If the complete condensation assumption is made, RHEED intensity would be directly proportional to the step migration velocity. And we tried to draw the Arrhenius plot for the RHEED intensity. The result was obtained with activation energy of 1.0 eV, as shown in Fig. 4-5[10].
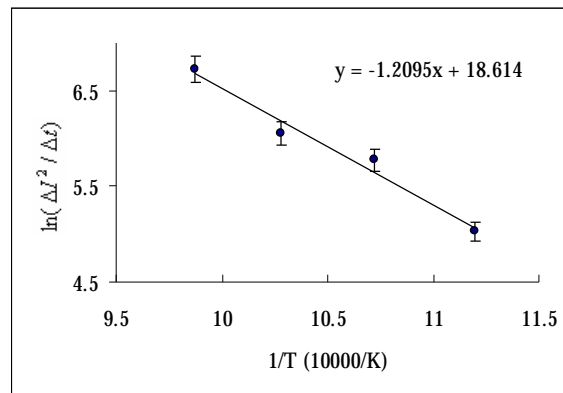
Fig. 4-5. Diffusion Arrhenius plot of $\ln(\Delta I^2 / \Delta t)$ vs. 1/T. Activation energy of 1.0 eV can be obtained. Combined with the step migration assumption, this energy level strongly suggests that certain atomistic barrier-crossing mechanism can be revealed directly from RHEED monitoring.

Due to the undefined proportion factor between the step edge density and the RHEED intensity, the diffusion coefficients of corresponding temperatures would not be explicitly obtained. However the activation energy of the order of atomistic barriers suggests that under well-controlled diffraction condition and proper film environment, the RHEED intensity may directly provide useful information on kinetic analysis.

In summary, following the step edge model we conducted a series of in-situ RHEED intensity investigations on the interrupted deposition of STO epitaxial films. Recovery of the RHEED intensity at various temperatures provided kinetic information for the grain boundary dislocation diffusion, for which activation energy of 1.0 eV was obtained from the diffusion Arrhenius plot with the diffusion length assumed to be proportional to the RHEED intensity.

In the previous section we have obtained the activated diffusion characteristics from the study of constant temperature annealing on relatively flat STO epitaxial films. For investigating the high defect density limit, a series of in situ RHEED monitored rising temperature annealing experiments have been conducted on room temperature deposited films[11].

The STO thin films were grown on four different substrates at room temperature. The same amount material of STO by 500 laser pulses was deposited on each substrate, and then the different constant heating rates are used to anneal the films. All four curves of RHEED intensity immediately drop deeply and maintain the constant minimum value without oscillation till the time of the laser-off, as in Fig. 4-6.
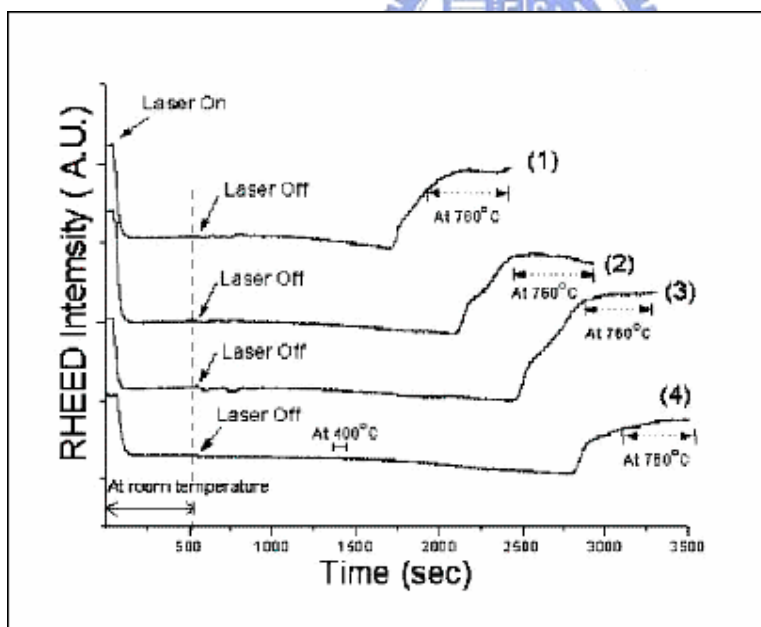

Fig. 4-6. RHEED intensity of annealed STO film with different heating rates. (1) for 35°C/min, (2) for 25°C/min and (3)for 20°C/min. (4) experienced 25°C/min to 400°C, held for 60 seconds and then heated to 760°C with the rate 15°C/min.

The diffraction spots disappear very quickly when laser was turned on at room temperature revealing that the coverage of the growing surface is at a minimum value and/or small islands were distributed on the electron-diffracting plane. After the laser was turned off, the substrate heater is turned on and the substrate temperature was monotonically increased toward 760°C with different constant rising rates.

All RHEED intensities of the annealed films showed a sudden rise at a narrow temperature range starting from 660°C, as can be identified from the temperature curves of Fig. 4-7.
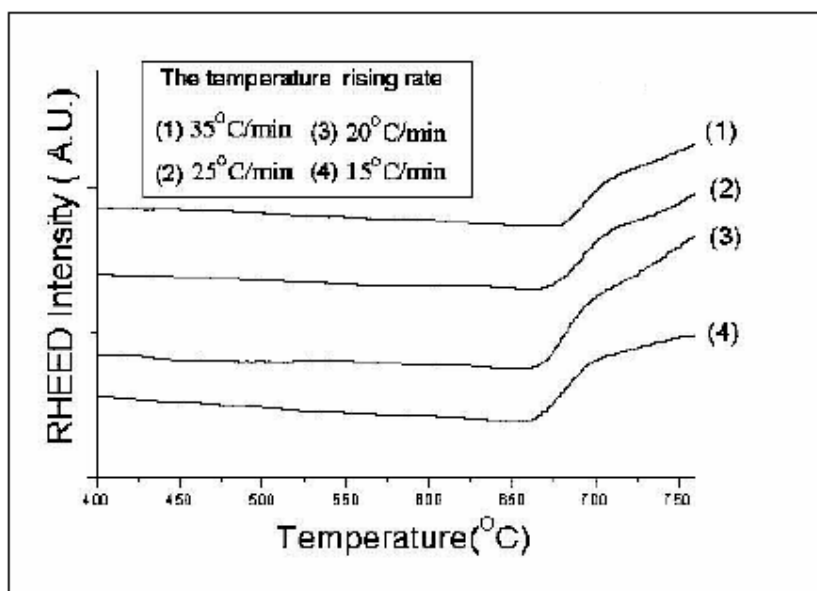

Fig. 4-7. The temperature dependence of RHEED intensity rescaled from Fig. 4-6.

This temperature annealing result revealed two significant features. First to be noticed is the temperature threshold for the sudden appearance of the RHEED. The other is the following decay of the rising rate of RHEED. For more information on the

57

rising intensity, the first order temperature derivative curves can be drawn as shown in Fig. 4-8.
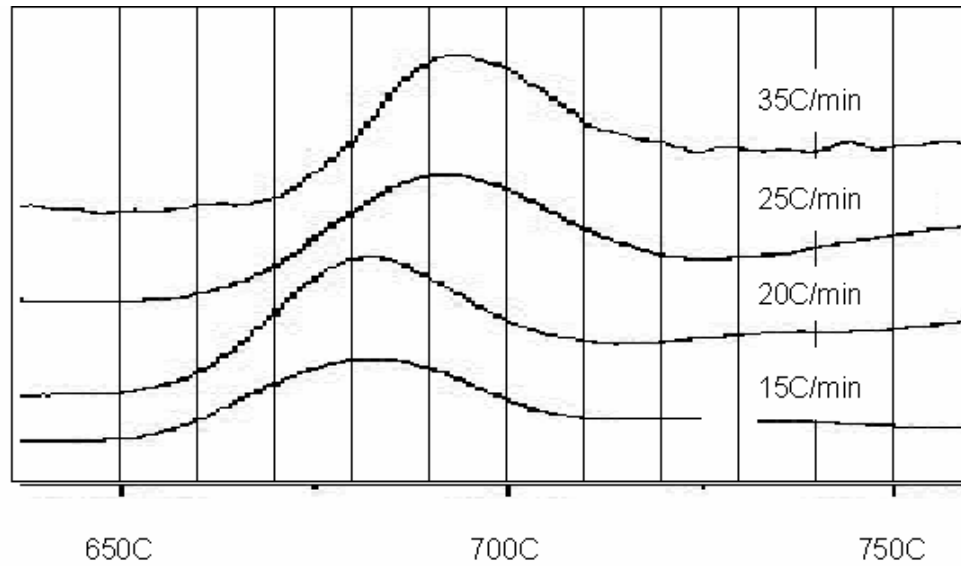

Fig. 4-8. Temperature dependence curves of the derivative RHEED intensity of different heating rates. Peak temperatures can be obtained as 693°C, 691°C, 682°C and 681°C for heating rates of 35, 25, 20 and 15°C/min respectively.

We noticed a differential thermal analysis method for calculating activation energy from the peak shift of different heating rate was originally developed by Kissinger[6]. By designating the heating rate as a, the peak temperature of the differential intensity as T_p, an activation energy can be obtained from the product of the gas constant and the slop of the Kissinger plot of $\ln(a/T_p^2)$ versus $1/T_p$ if we take the temperature annealing RHEED intensity as the reaction variable considered in Kissinger's DTA method. From the Kissinger plot of peak temperature shift, the activation energy of 4 eV is obtained.

This activation energy is apparently higher than the activation energy of the

diffusion barrier of the smooth films with dilute defects. We may consider another mechanism for this abrupt smoothening phenomenon. The larger activation energy suggests that there are two different energy barriers during the interrupted deposition. The first one with higher activation energy of 4 eV may be attributed to certain smoothening transition of high dislocation density. The second mechanism with energy barrier of 1 eV can be considered as the evolution of isolated dislocation at low defect density.
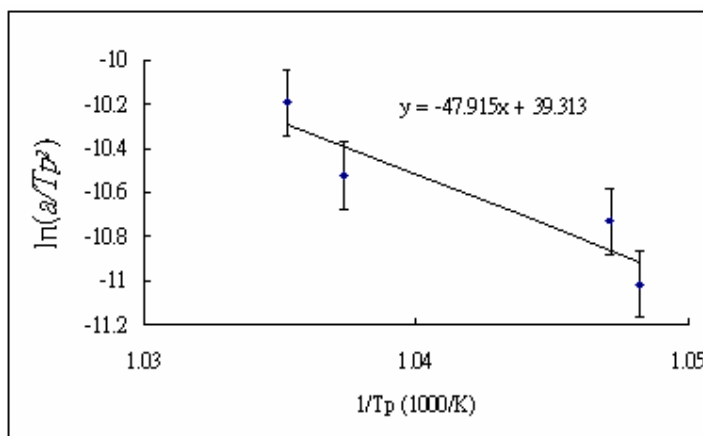

Fig. 4-9. Kissinger plot from the differential RHEED intensity of heating rates of 35, 25, 20 and 15°C/min respectively. From multiplying the slop with the gas constant, approximately 4eV is obtained as the activation energy.

To explain this RHEED-temperature annealing behavior, we can have two representations. First is from the surface morphology point of view. Considering the roughness of the room-temperature deposited film and the deep drops of the RHEED intensity when laser was on, the sudden recovery above 660°C apparently indicates a more efficient surface smoothening process. It's likely this process is resulted from near interaction of dislocations in high defect density condition. While the lower activation energy result implies a gentle grain growth mechanism in a dilute defect

59

sample. The isolated islands coalescence through atomistic diffusion may be responsible for this stage of RHEED recovery.

Besides the geometrical interpretation of the temperature annealing behavior shown in Fig. 4-9 to Fig. 4-8, an averaged dynamic model of Langevin equation like formulism has also been considered[11].

We chose to start from an averaged equation of motion of Langevin type for Brownian motion [See Appendix 2]
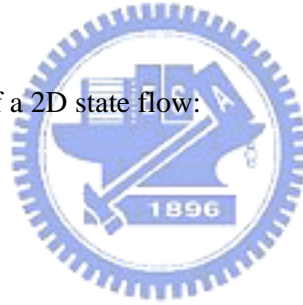
$$m\frac{d^2x(t)}{dt^2} = -z\frac{dx(t)}{dt} + F(t).$$

The force balance equation for the averaged displacement of the step edges can be assumed to be directly proportional to the RHEED intensity in the previous section:

$$m\frac{d^2\bar{x}}{dt^2} = -b\bar{v} - k\bar{x} + gt - F_d \qquad (18)$$

or alternatively in the form of a 2D state flow:

$$\bar{v} = \frac{d\bar{x}}{dt}, \qquad (19)$$

$$m\frac{d\bar{v}}{dt} = -b\bar{v} - k\bar{x} + gt - F_d$$

where $\bar{x}$ is defined as the averaged step edge displacement and the RHEED intensity, v is the velocity, k represents a spring constant, b represents the damping constant, F_d is defined as a dynamical friction force and gt is postulated to measure the temperature dependent "depinning" force which obeys the linear temperature proportionality as a flux line in the 2D creep model of Anderson and Kim[12]. The model can schematically presented as Fig. 4-10.
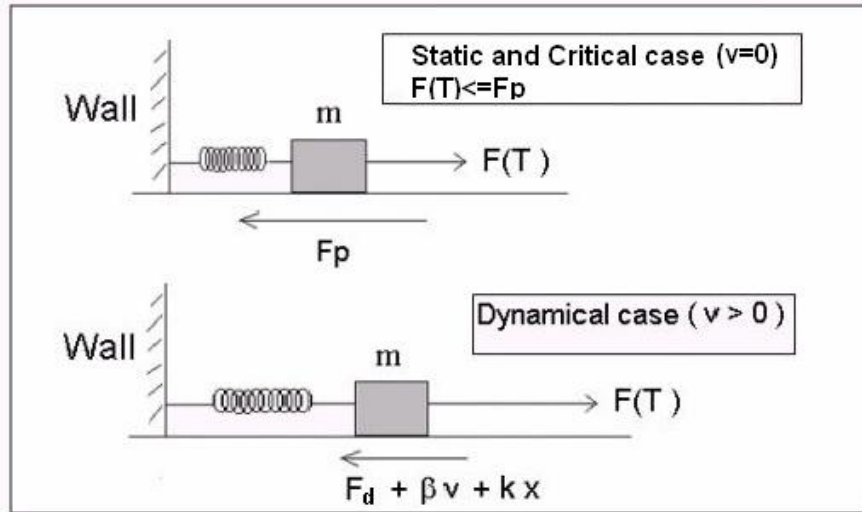
Fig. 4-10. Schematics of the Langevin-like averaged equation of motion governing

the step edge motion.

Qualitatively, below the temperature threshold or the initial stage of the time, one

considers the step edges are pinned by a static friction force or the pinning force Fp,

as shown in the upper part of the figure. Only above the critical temperature of about

660°C when the thermally activated depinning force F(T)=gt becomes larger than the

pinning force Fp, the model (19) or (20) can be simulated to show the averaged

motion of the step edges.

One of the results displaying good agreement between the simulated and

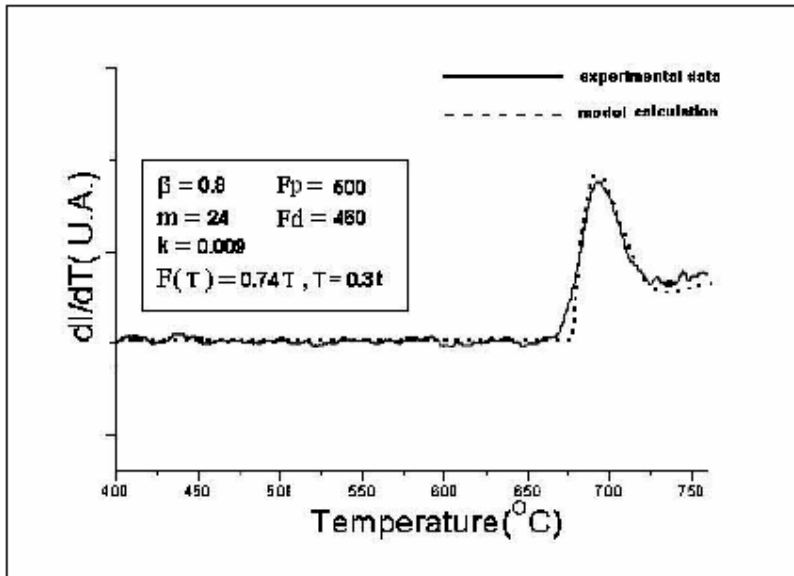measured RHEED intensity derivatives is shown in Fig. 4-11.

Fig. 4-11. A simulated and measured RHEED intensity derivative vs. temperature for

room temperature deposited films annealing.

In summary, from a series of RHEED monitored constant temperature annealing for the STO laser ablated Epitaxial films, we obtained an effective activation energy of 1eV from the Arrhenius plot of RHEED intensity squared with respect to annealing time. For another series of annealing with rising temperature for room temperature deposited films, an effective energy of 4 eV can be obtained from the Kissinger plot of peak temperature of differential RHEED intensity with respect to heating rate. Within the experimental error, the former barrier can be attributed to the kink site removing barrier of Strontium oxide or Titanium oxide in poorly crystallized STO films. And the latter may be caused by diffusion of atomistic species on relative flat surface of Epitaxial STO films. Both activated kinetic characteristics shed light on the pinning potential of the diffusion of surface defect. A Langevin-like force balance model for the RHEED phase is discussed. Preliminary numerical simulated result can be fitted into observed data. Hopefully more detailed verification both theoretical and experimental can be made to develop a better model to quantitatively interpret the RHEED intensity and its oscillation during Epitaxy deposition.

References

[1] J. J. Harris, B. A. Joyce, and P. J. Dobson, Surf. Sci. **103**, L90 (1981); ibid. **108**, L444 (1981); C. E. C. Wood, ibid. **108**, L441 (1981).

[2] J. H. Neave et al., Appl. Phys. **A 31**, 1 (1983).

[3] "RHEED and Reflection Imaging of Surfaces", edited by P. K. Larsen and P. J. Dobson (Plenum, New York, 1988), p. 427.

[4] For example, I.N. Levine, Physical Chemistry, McGraw-Hill, Boston, 1995, 4th ed.

[5] H.A. Kramers, Physica, **7**, 284 (1940).

[6] H.E. Kissinger, Analytical Chemistry **29**, 1702 (1957).

[7] L.C. Chen and F.J. Spaepen, J. Appl. Phys. **69**, 679 (1991).

[8] T. Franke, P. Kreutzer, Th, Zacher, W. Naumann and R. Anton, J. Crystal Growth, **193**, 451 (1998).

[9] J.H. Neave, P.J. Dobson, B.A. Joyce and Jing Zhang, Appl. Phys. Lett. **47** (2) 100 (1985).

[10] T.C. Wang, J.Y. Juang, K.H.Wu, T.M. Uen and Y.S.Guo Jap. J. Appl. Phys. 43, 771 (2004).

[11] J.Y. Lee, doctoral dissertation, national Chiao-Tung University, Taiwan, 2001.

[12] "Introduction to Superconductivity, 2nd edition", Michael Tinkham, Mcgraw-Hill, Singapore, 180 (1996).

Chapter 5   Concluding Remarks

After reviewing the dissipated and driven nonlinear oscillation, a collective macroscopic quantum phase locking picture was suggested for the unifying framework of the devil's staircase fractal structure of driven Josephson oscillation and the quantized Hall effects.

A direct proportionality between the interrupted RHEED intensity oscillation and the averaged defect length has been proposed to describe the kinetic characteristics of the thermally activated diffusion of laser ablated Epitaxial film growth.

In the first part of the dissertation, the macroscopic Josephson voltage frequency relation has been considered as a de Broglie energy frequency relation. Focusing on the dissipative phase locking mechanism, the discrete time nonlinear dynamical system formulated by the Resistively and Capacitively Shunted Junction model was pointed out as a candidate capable of connecting the driven Josephson ac effect and the Quantized Hall effects. The macroscopic phase-locking quantization scenario is suggested to provide a common dynamic framework with a fractal Hall curve for IQHE and FQHE.

In the second part of the dissertation, while examining the oscillating RHEED intensity we find the first time that the thermally activated diffusion kinetics can be characterized directly by the RHEED intensity.

The Arrhenius plot from the interrupted deposition RHEED intensity recovery for the epitaxial films provided the activation energy of 1 eV of isolated line defect evolution and atomistic diffusion for the flat film corresponding the oscillation peaks of RHEED intensity. The Kissinger plot of RHEED intensity of annealing with different constant heating rate was drawn for room temperature deposited films. The activation energy of 4 eV obtained from the Kissinger plot suggested an abrupt

smoothening behavior in poorly crystallized STO films, which may be related to the island coalescence corresponding to the bottoms of a RHEED oscillation.

From the diffusion point of view, a Langevin-like averaged force equation is reviewed for modeling the depinning-like behavior of the annealing experiments. One of the inspiring concepts capable of bridging the gap between the macroscopic oscillatory behavior, quantum or classical, and microscopic particles may be found in the "order parameter". In the collective quantum oscillation displayed by the RCSJ equation, the condensed phase can be considered as a thermodynamic Ginzberg-Landau order parameter as well as a quantum dynamical variable. In the thermally activated dislocation evolution problem, the defect length or the diffusion displacement may be regarded as playing a similar role in the Langevin force balanced equation.

Appendix:

1. Nonlinear Oscillation and Phase Space Evolution

A nonlinear oscillator is described typically in the form of a second order ordinary differential equation such as

$$\ddot{x} + a\dot{x} + w_0^2 x + bx^3 = f \sin wt, (\cdot = \frac{d}{dt}) \tag{1}$$

which is the well-known Duffing oscillator[1] with b defining the strength of the nonlinearity. In the undamped $(a = 0)$ and unforced $(f = 0)$ situation, the equation can be solved analytically with the Jacobian elliptic functions. For instance, when $w_0^2 > 0, b > 0$ the solution can be exactly expressed as:

$$x(t) = A\mathrm{cn}(vt), v = \sqrt{(w_0^2 + bA^2)}, \tag{2}$$

where cn represents the Jacobian elliptic function. The periodic variation of x with respect to time can be seen from Fig. A-1.
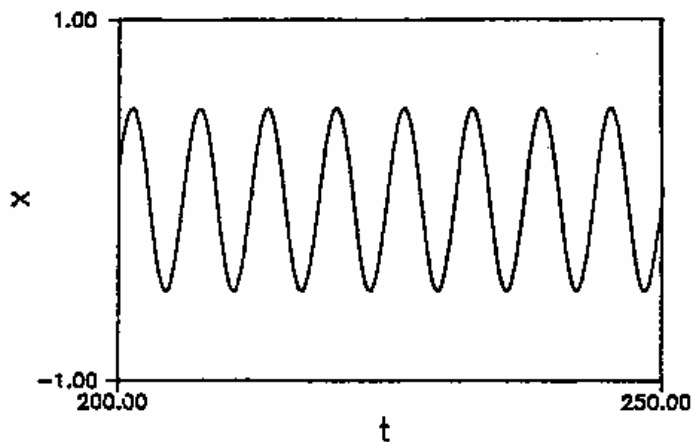

Fig. A-1. Analytical time evolution of the Duffing equation without damping and

driven force.

One can alternatively present the solution in the form of phase portrait, as Fig. A-2.
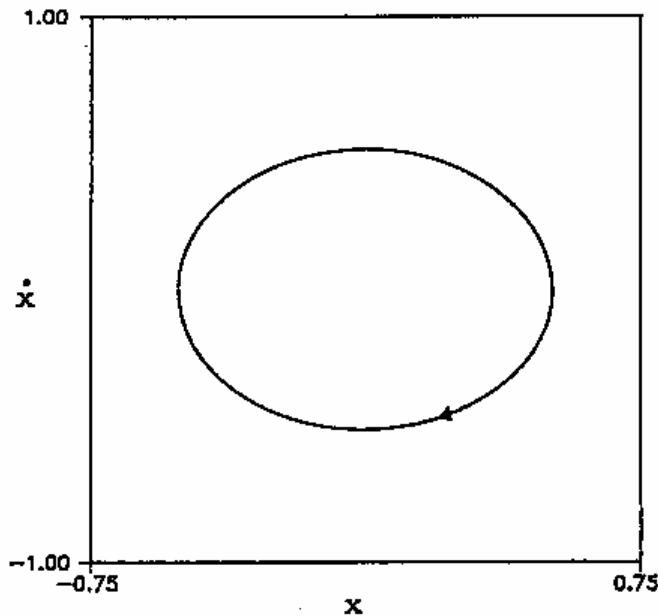

Fig. A-2. The phase portrait representation of the solution (2) of Duffing equation.

In the parameter region of $a > 0$, the damped oscillation can be illustrated by a inwardly spiraling trajectory in the phase portrait as shown in Fig. A-3.

With the nonlinearity from the cubic term bx^3 in equation (1), the Duffing oscillator displays qualitatively different features compared to the linear case with $b = 0$. For example, Fig. A-4. shows a typical resonance curve of small nonlinearity.
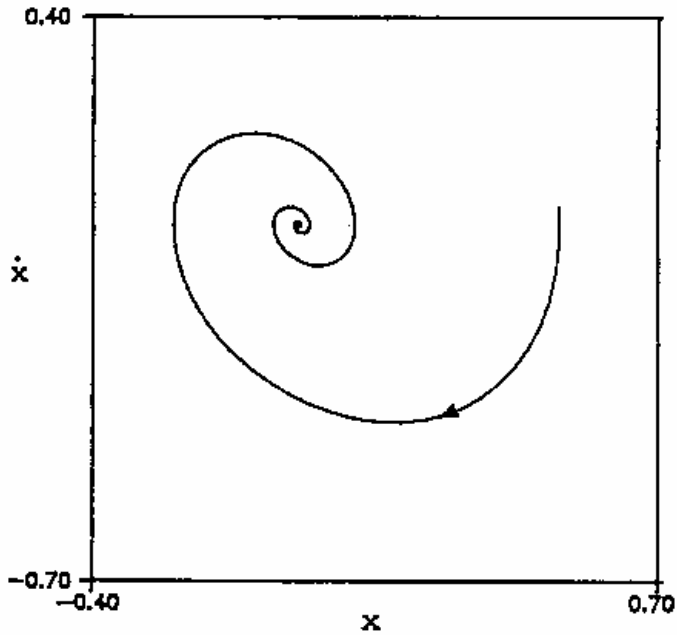
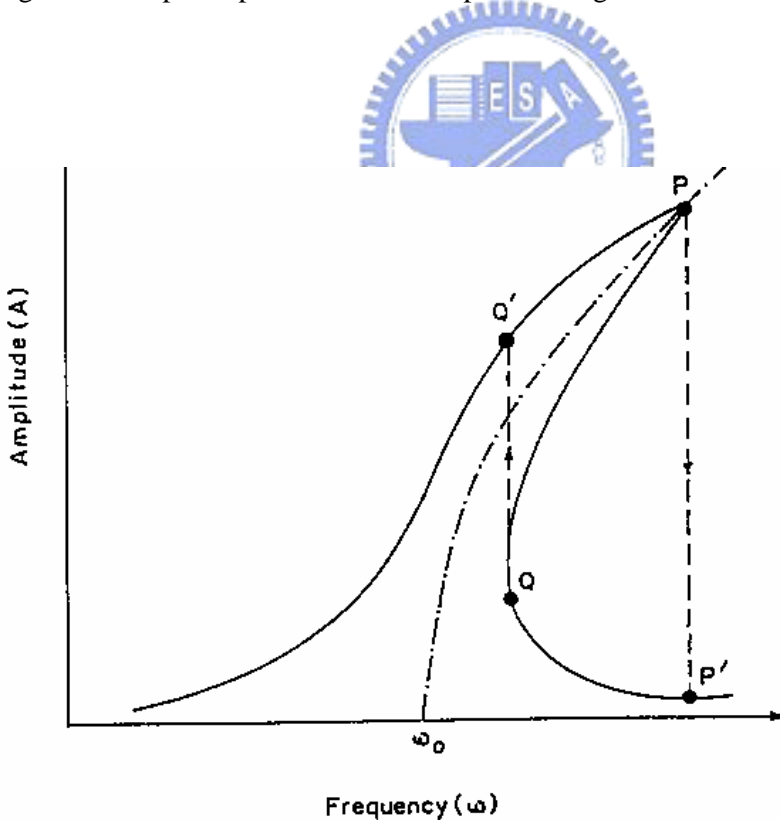Fig. A-3. The phase portrait of the damped Duffing oscillation.

Fig. A-4. Resonance curve of the Duffing oscillator with small nonlinearity.

69

The key feature different from the linear case can be seen from the bell-shaped curve with asymmetry. This asymmetry directly results in the discontinuous jump and hysteresis. Starting from the point Q', the oscillation amplitude increases gradually with the increasing frequency of the driving force just like in a linear system. When it arrives at the peak P however, the amplitude suddenly drops to P' under a small increase in the driving frequency. The similar situation happens during the frequency decreasing from the point Q to Q'.

This example analytically demonstrates only a part of basic nonlinear dynamical behaviors. In general this equation is not exactly solvable. Numerical integration armed with high speed computing is capable of exploring a much richer variety of nonlinear phenomena. These phenomena can be analyzed through the following non analytical tools:

1. Trajectory plot: the plot of x(t).

2. Phase portrait: the 2D projection of the trajectories in the $(x, \dot{x})$ phase plane. Periodicity can be directly identified from this representation.

3. Poincaré map: for driven non-autonomous system, the map is the stroboscopic or the snap-shot portrait of the phase space trajectories at every period of the driving force. Periodic solution will be revealed by finite number of points in this sectioning map, while complex or chaotic behavior can appear as a fractal attractor.

4. Bifurcation diagram: the sectioned state point value versus a control parameter. Can be used to reveal the period doubling or other bifurcation routes from periodic to chaotic region.

5. Lyapunov exponent: the exponential measure of attraction or separation with respect to time of two adjacent trajectories in phase space.

A non-autonomous driven second order equation of motion as (1) can be rewritten as a set of three first order equations:

$$\dot{x} = y,$$
$$\dot{y} = -ay - w_0^2 x - bx^3 + f \sin z \qquad (3)$$
$$\dot{z} = w.$$

This phase evolution expression of the three dimensional dynamical system can be regarded as the "cleanest form" of the periodically driven oscillation, linear or nonlinear. A stroboscopic Poincaré section can reveal all kinds of the permanent or asymptotic behaviors in this system.

The steady states appear in the sectioned 2D phase space consists of:

(a) Fixed point: represents the fixed state remains unchanged as time evolves.

(b) Period response including subharmonic and superharmonic response: solutions resonating with the driving force by an integer or fractional frequency ratio.

(c) Quasiperiodic: solutions made up with periodic components of incommensurable fundamental frequencies, i.e., irrational frequency ratio.

(d) Chaotic response: phase points evolve more and more distant from each other exponentially with respect to time, final condition is always sensitively dependent on initial condition.

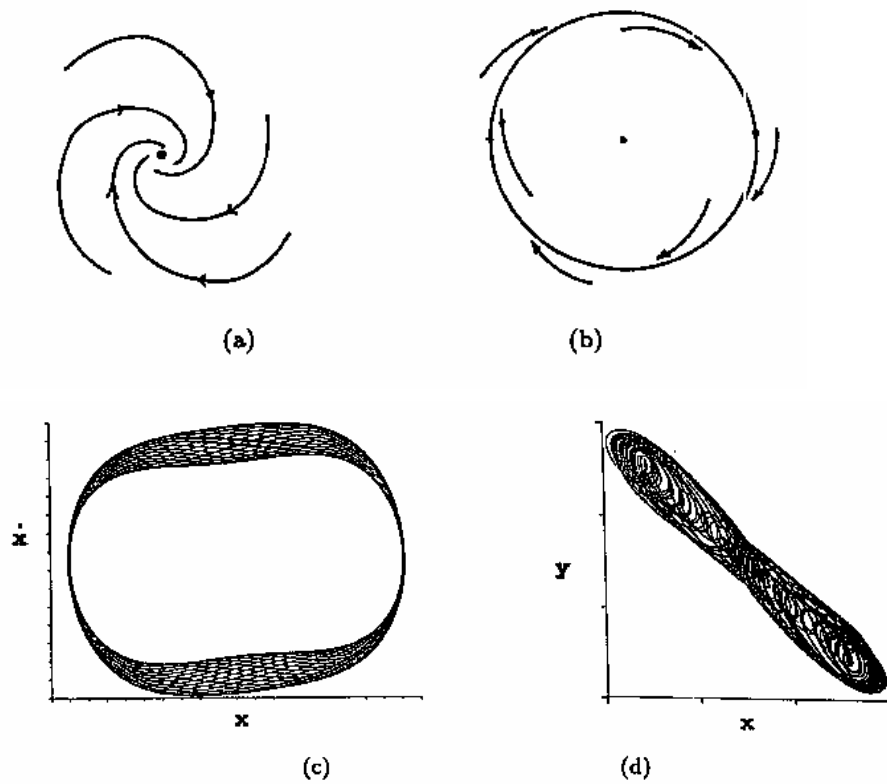Typical examples of these situations can be found in Fig. A-5.

Fig. A-5. Stroboscopically sectioned phase portraits of the dynamical state evolution:

(a) fixed state, (b) periodic state, (c) quasiperiodic state and (d) chaotic state.

Reference

[1] G. Duffing, *Erzwungene Schwingungen bei Veränderlicher Eigen Frequenz und ihre Technische Bedeutung* (Vieweg, Brauschweig, 1918).

2. Surface Diffusion and Brownian Motion Modeled by Langevin Equation

Diffusion on the solid surface has been attracting attention since the early development of molecular beam epitaxy technology[2]. The diffusion coefficient D_s of an atom on a solid surface may be defined as

$$2mD_s t = <|r(t) - r(0)|^2>,\tag{1}$$

where m is the space dimensionality of the migration, t the time period of observations and r the position vector of the adatom. The average is taken from repeated observations of the same time period t.

The average number of jumps in a time period is traditionally written as the Arrhenius equation:

$$\overline{N} = n_0 t \exp(-E_d / kT),\tag{2}$$

n_0 is the effective frequency factor of the atomic jumps and E_d is the activation energy of surface diffusion or the barrier height of the atomic jumps. Assuming the adatoms move according to the nearest neighbor random walks, the mean square displacement can be proved to follow the famous relation:

$$<(\Delta x)^2> = Nl^2,\tag{3}$$

where l is the nearest-neighbor distance. From equations (1), (2) and (3) we have

$$D_s = \frac{<(\Delta r)^2>}{2mt} = D_0 \exp(-E_d / kT),\tag{4}$$

where $D_0 = n_0 l^2 / 2m$. It is therefore clear that one can obtain the diffusion coefficient and the activation energy by equation (4) as long as the mean square displacement and the hopping time were measured. This formulism is a typical method to get the activation energy of atomistic diffusion barriers.

There are several approaches to get the result of equation (1), which correlates the macroscopic transport quantity, i.e., diffusion coefficient, with the averaged microscopic dynamic quantity hopping time and length. The Langevin Equation provided an intuitive picture to model the random walk of atoms[3].

The force equation of a Brownian particle can be written as

$$m\frac{d^2x(t)}{dt^2} = -z\frac{dx(t)}{dt} + F(t),\tag{5}$$

where z represents the dissipation or the viscous interaction in a fluid and the $F(t)$ defines the random force of the environment. Langevin transformed the stochastic equation into an analytically solvable problem by starting with multiplying (5) with x:

$$m\ddot{x}x = -z\dot{x}x + F(t)x.\tag{6}$$

Considering

$$\dot{x}x = \frac{1}{2}\frac{d}{dt}(x^2),\tag{7}$$

and

$$\ddot{x}x = \frac{1}{2}\frac{d}{dt}\left(\frac{d(x^2)}{dt}\right) - \dot{x}^2,\tag{8}$$

he obtained

$$\frac{m}{2}\frac{d}{dt}\left(\frac{dx^2}{dt}\right) - m\dot{x}^2 = -\frac{z}{2}\frac{dx^2}{dt} + F(t)x.\tag{9}$$

This equation describes a single Brownian particle. Taking an ensemble average for the equation of motion, we have

$$\frac{m}{2}\frac{d}{dt}\left(\frac{\overline{dx^2}}{dt}\right) - m\overline{\dot{x}^2} = -\frac{z}{2}\frac{\overline{dx^2}}{dt} + \overline{F(t)x}.\tag{10}$$

Besides the mean square displacement $\overline{x^2}$, the averaged multiplication of the random force and the displacement $\overline{F(t)x}$ is assumed to vanish since the irregular motion is uncorrelated to the displacement. If the maxwellian distribution is assumed to be

applied, the second averaged kinetic energy term of (10) can be replaced by

equipartition relation

$$\frac{1}{2}m\overline{\dot{x}^2} = \frac{1}{2}kT \tag{10a}$$

and the averaged equation of motion can be rewritten as

$$\frac{m}{2}\frac{d}{dt}(\frac{d\overline{x^2}}{dt}) + \frac{z}{2}\frac{d\overline{x^2}}{dt} = kT. \tag{11}$$

If a new variable u is defined as

$$\frac{d\overline{x^2}}{dt} = u, \tag{12}$$

the equation is reformed as

$$\frac{m}{2}\frac{du}{dt} + \frac{z}{2}u = kT. \tag{13}$$

The analytical solution can be expressed as

$$u = \frac{2kT}{z} + Ce^{-(z/m)t}. \tag{14}$$

When the time scale is large compared to the ratio m/z, or the inertia of the

Brownian particle can be ignored, the solution can be further reduced to

$$u = \frac{d\overline{x^2}}{dt} = \frac{2kT}{z}. \tag{15}$$

Or represented in an integrated form as

$$\overline{x^2} - \overline{x_0^2} = \frac{2kT}{z}t \tag{16}$$

or

$$\overline{(\Delta x)^2} = \frac{2kT}{z}t. \tag{17}$$

One can easily obtain the space-time relation for random walk (1) simply defines

$$\frac{kT}{z} = mD \tag{18}$$

where m represents the space dimensionality of the diffusion and D the diffusion

coefficient.

Biographical Notes

Personal Data

Name　　　　: Te-Chun Wang

Sex　　　　: Male

Date of Birth : December 30, 1962

Education

1981/09 – 1985/07　National Taiwan University, Taipei, Taiwan

　　　　　　　　　BS degree in Chemical Engineering

1989/09 – 1991/07　National Cheng-Kung University, Tainan, Taiwan

　　　　　　　　　MS degree in Material Science and Engineering

1994/09 – 2004/07　National Chiao-Tung University, Hsinchu, Taiwan

　　　　　　　　　Ph.D degree in ElectroPhysics

Publication List

1. T. C. Wang, J. Y. Lee, C. C. Hsieh, J. Y. Juang, K. H. Wu, T. M. Uen and Y. S. Gou, "Activated Kinetics of Room Temperature Deposited SrTiO3 Thin Films Investigated by Reflection High Energy Electron Diffraction Monitored Annealing with Different Heating Rates", Japanese Journal of Applied Physics (2004) in press.

2. T. C. Wang, J. Y. Lee, J. Y. Juang, K. H. Wu, T. M. Uen and Y. S. Gou, "RHEED in-situ Monitored Step Edge Diffusion During Interrupted Laser Ablation Epitaxy Growth of SrTiO3", Chinese Journal of Physics (2004) in press.

3. T.C. Wang, J.Y. Juang, K.H. Wu, T.M. Uen and Y.S. Gou, "Thermally activated diffusion observed by in-situ RHEED intensity monitoring on interrupted SrTiO3 homoepitaxial growth", Japanese Journal of Applied Physics(Part I), 43, 771 (2004).

4. J. Y. Lee, T. C. Wang, S. F. Chen, J. Y. Juang, J. Y. Lin, K. H. Wu, T. M. Uen and Y. S. Gou, "Growth Kinetics of Homoepitaxial Strontium Titanate Films by Interrupted Pulsed Laser Deposition", Chinese Journal of Physics, 39, 4, L300 (2001).

5. T.C. Wang and Y.S Gou, "A Discussion on the Josephson AC Effect and the Fractional Energy Quantization", Chinese Journal of Physics, 34, 2-II, 665 (1996).